



HAL
open science

Non-canonical mTOR-Independent Role of DEPDC5 in Regulating GABAergic Network Development

Amrutha Swaminathan, Rahma Hassan-Abdi, Solène Renault, Aleksandra Siekierska, Raphaëlle Riché, Meijiang Liao, Peter de Witte, Constantin Yanicostas, Nadia Soussi-Yanicostas, Pierre Drapeau, et al.

► **To cite this version:**

Amrutha Swaminathan, Rahma Hassan-Abdi, Solène Renault, Aleksandra Siekierska, Raphaëlle Riché, et al.. Non-canonical mTOR-Independent Role of DEPDC5 in Regulating GABAergic Network Development. *Current Biology - CB*, 2018, 28 (12), pp.1924-1937.e5. 10.1016/j.cub.2018.04.061 . hal-02364352

HAL Id: hal-02364352

<https://hal.science/hal-02364352>

Submitted on 14 Nov 2019

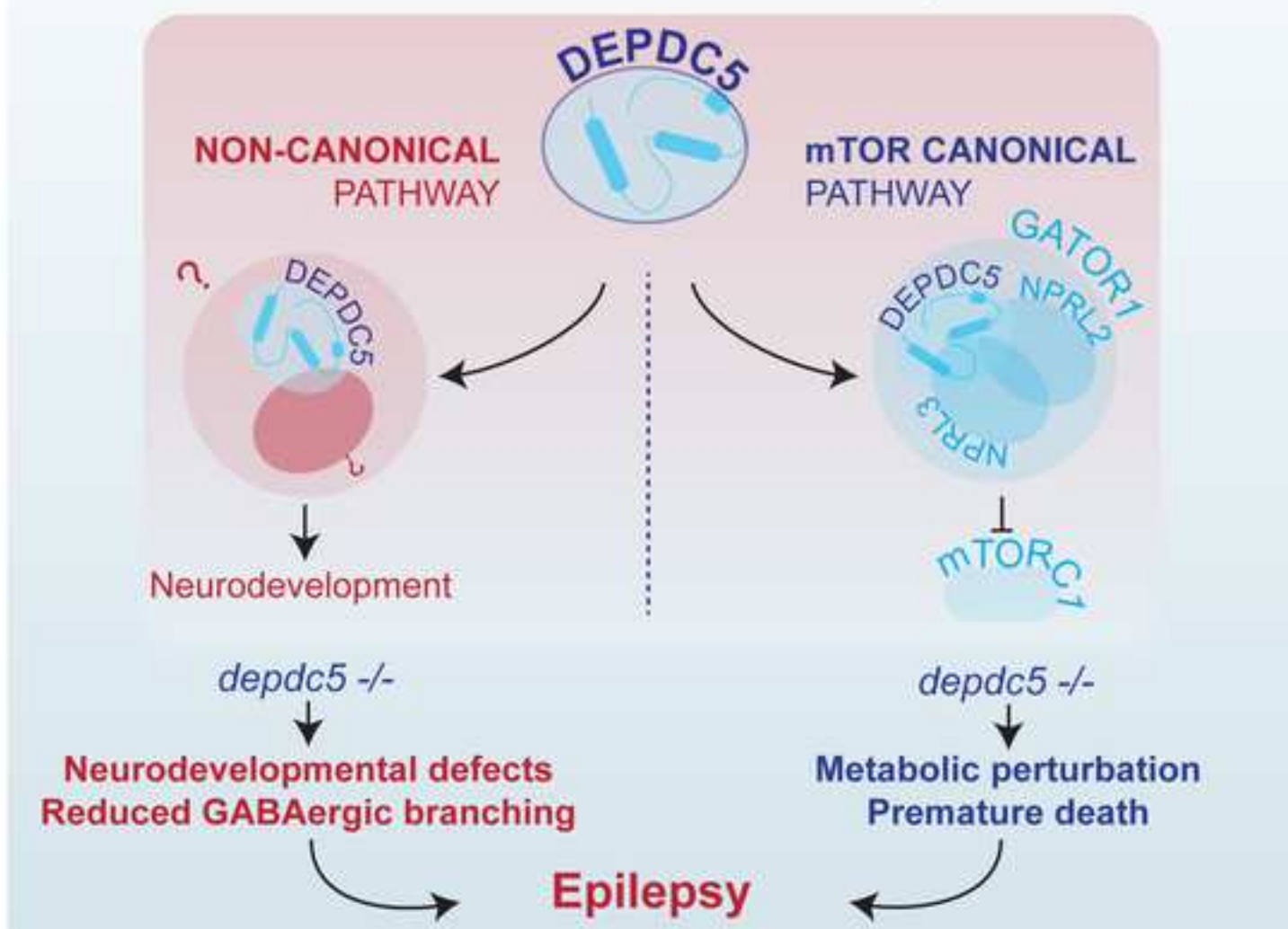
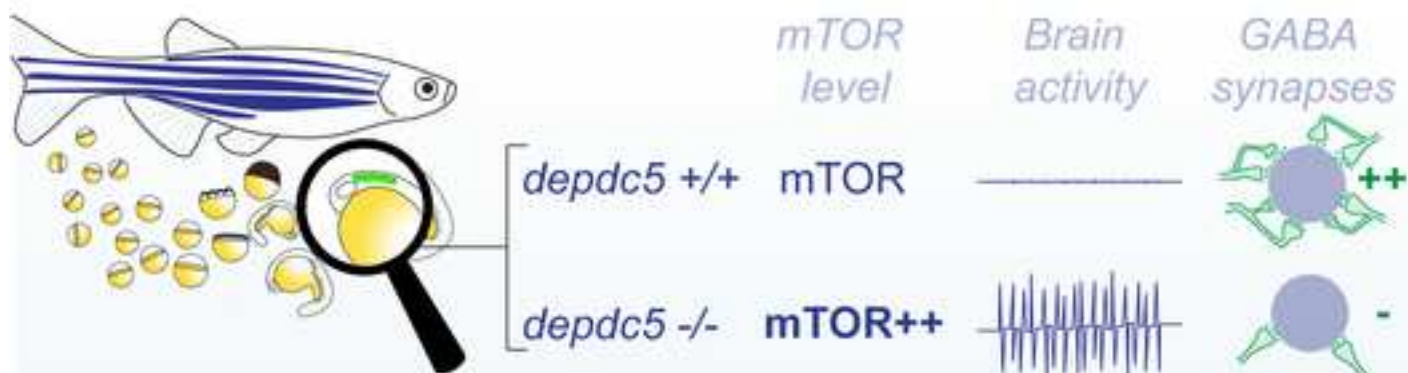
HAL is a multi-disciplinary open access archive for the deposit and dissemination of scientific research documents, whether they are published or not. The documents may come from teaching and research institutions in France or abroad, or from public or private research centers.

L'archive ouverte pluridisciplinaire **HAL**, est destinée au dépôt et à la diffusion de documents scientifiques de niveau recherche, publiés ou non, émanant des établissements d'enseignement et de recherche français ou étrangers, des laboratoires publics ou privés.

Current Biology

Non-canonical mTOR-independent role of DEPDC5 in regulating GABAergic network development --Manuscript Draft--

Manuscript Number:	CURRENT-BIOLOGY-D-17-01554R3
Full Title:	Non-canonical mTOR-independent role of DEPDC5 in regulating GABAergic network development
Article Type:	Research Article
Corresponding Author:	Eric Samarut, Ph.D CRCHUM Montreal, CANADA
First Author:	Amrutha Swaminathan
Order of Authors:	Amrutha Swaminathan Rahma Hassan-Abdi Solene Renault Aleksandra Siekierska Raphaelle Riche Meijiang Liao Peter A.M de Witte Constantin Yanicostas Nadia Soussi-Yanicostas Pierre Drapeau Eric Samarut, Ph.D
Abstract:	<p>Mutations in DEPDC5 are causal factors for a broad spectrum of focal epilepsies, but the underlying pathogenic mechanisms are still largely unknown. To address this question, a zebrafish <i>depdc5</i> knockout model showing spontaneous epileptiform events in the brain, increased drug-induced seizure susceptibility, general hypoactivity and premature death at 2-3 weeks post fertilization as well as the expected hyperactivation of mTOR signaling was developed. Using this model, the role of DEPDC5 in brain development was investigated using an unbiased whole transcriptomic approach. Surprisingly, in addition to mTOR-associated genes, many genes involved in synaptic function, neurogenesis, axonogenesis and GABA network activity were found to be dysregulated in larval brains. Although no gross defects in brain morphology/neuron loss were observed, immunostaining of <i>depdc5</i>^{-/-} brains for several GABAergic markers revealed specific defects in the fine branching of GABAergic network. Consistently, some defects in <i>depdc5</i>^{-/-} could be compensated by treatment with GABA, corroborating that GABA signaling is indeed involved in DEPDC5 pathogenicity. Further, the mTOR-independent nature of the neurodevelopmental defects was demonstrated by the inability of rapamycin to rescue the defects of GABAergic networks observed in <i>depdc5</i>^{-/-} brains and conversely, the inability of GABA to rescue the hypoactivity in another genetic model showing mTOR hyperactivation. This study hence provides the first in vivo evidence that DEPDC5 plays previously unknown roles apart from its canonical function as an mTOR inhibitor. Moreover, these results propose that defective neurodevelopment of GABAergic network could be a key factor in epileptogenesis when DEPDC5 is mutated.</p>



1 **Non-canonical mTOR-independent role of DEPDC5 in regulating GABAergic**
2 **network development.**

3
4 Amrutha Swaminathan¹, Rahma Hassan-Abdi^{2,3}, Solène Renault^{2,3}, Aleksandra Siekierska⁴,
5 Raphaëlle Riché¹, Meijiang Liao¹, Peter A.M. de Witte⁴, Constantin Yanicostas^{2,3}, Nadia Soussi-
6 Yanicostas^{2,3}, Pierre Drapeau^{1,5#} and Éric Samarut^{1,5.#}

7
8 ¹ Department of Neurosciences, Research Center of the University of Montréal Hospital Center
9 (CRCHUM), Université de Montréal, Montréal, Canada H2X0A9.

10 ² Inserm, U1141, F-75019 Paris, France

11 ³ Université Paris Diderot, Sorbonne Paris Cité, UMRS 1141, F-75019 Paris, France

12 ⁴ Laboratory for Molecular Biodiscovery, Department of Pharmaceutical and Pharmacological
13 Sciences, University of Leuven, 3000 Leuven, Belgium

14 ⁵ DanioDesign Inc., Montréal, Canada.

15 # Co-corresponding authors: p.drapeau@umontreal.ca and eric.samarut@umontreal.ca

16 Lead contact: Éric Samarut (eric.samarut@umontreal.ca)

17

18

19 **Running title:** DEPDC5 regulates GABA network development

20

21

22 **Summary**

23 Mutations in *DEPDC5* are causal factors for a broad spectrum of focal epilepsies, but the
24 underlying pathogenic mechanisms are still largely unknown. To address this question, a
25 zebrafish *depdc5* knockout model showing spontaneous epileptiform events in the brain,
26 increased drug-induced seizure susceptibility, general hypoactivity, premature death at 2-3 weeks
27 post fertilization as well as the expected hyperactivation of mTOR signaling was developed.
28 Using this model, the role of DEPDC5 in brain development was investigated using an unbiased
29 whole transcriptomic approach. Surprisingly, in addition to mTOR-associated genes, many genes
30 involved in synaptic function, neurogenesis, axonogenesis and GABA network activity were
31 found to be dysregulated in larval brains. Although no gross defects in brain morphology/neuron
32 loss were observed, immunostaining of *depdc5*^{-/-} brains for several GABAergic markers
33 revealed specific defects in the fine branching of GABAergic network. Consistently, some
34 defects in *depdc5*^{-/-} could be compensated for by treatment with GABA, corroborating that
35 GABA signaling is indeed involved in DEPDC5 pathogenicity. Further, the mTOR-independent
36 nature of these neurodevelopmental defects was demonstrated by the inability of rapamycin to
37 rescue the GABAergic network defects observed in *depdc5*^{-/-} brains and conversely, the inability
38 of GABA to rescue the hypoactivity in another genetic model showing mTOR hyperactivation.
39 This study hence provides the first *in vivo* evidence that DEPDC5 plays previously unknown
40 roles apart from its canonical function as an mTOR inhibitor. Moreover, these results propose
41 that defective neurodevelopment of GABAergic networks could be a key factor in
42 epileptogenesis when *DEPDC5* is mutated.

43

44 **Keywords:** Epilepsy/DEPDC5/GABA/mTOR/Neurodevelopment/zebrafish

45 **Introduction:**

46 Focal seizures, which originate in one part of the brain, are the most prevalent type of
47 epileptic seizures and mutations in *DEPDC5* (Dishevelled, Egl-10 and Pleckstrin (DEP)-domain
48 containing 5) account for 12-37% of the cases [1]. Though numerous ion channel mutations have
49 been traditionally associated with epilepsy, recent work using whole genome/exome sequencing
50 has identified other pathways in epilepsy, like mTOR (mechanistic/mammalian target of
51 rapamycin) signaling. The causative gene for familial focal epilepsy with variable foci (FFEVF)
52 remained unknown until the identification of *DEPDC5* mutations in a large number of families
53 with FFEVF [2-4]. Mutations in *DEPDC5* leading to haploinsufficiency have been associated
54 also to other focal epilepsies including autosomal dominant nocturnal frontal lobe epilepsy and
55 familial temporal lobe epilepsy [3, 5].

56 *DEPDC5*, along with *NRPL2* and *NRPL3* forms the mTOR inhibitory GATOR1
57 complex, which blocks the activation of the classical mTOR complex, mTORC1, when amino
58 acid concentration is low [6]. Mutations in all three components have been linked to focal
59 epilepsy with/without cortical malformations [7-10]. The mTOR pathway plays a significant role
60 in the regulation of protein synthesis and in critical cell fate decisions like autophagy. Absence of
61 regulation of this pathway results in constitutively high mTORC1 activity, and mTOR
62 hyperactivation has been implicated in various neurological conditions associated with
63 intractable seizures [11]. Thus, mTOR inhibitors like rapamycin and its analogs hold significant
64 potential in anti-epileptogenic therapies [12, 13].

65 Since the components of the GATOR1 complex have only been recently associated with
66 epilepsy, their pathophysiological roles related to focal epilepsy are yet to be completely
67 understood. Moreover, some initial discoveries found that multiple *DEPDC5* mutations in

68 patients are located in a domain of unknown function (DUF3608) [3], thus suggesting that
69 unexpected roles of DEPDC5 may be associated with its pathogenicity. There are three rodent
70 models of DEPDC5 knockout, where homozygotes show mTOR hyperactivation, severe
71 morphological defects and premature death [14-16]. The conditional knockout mouse model
72 reported recently describes cortical defects and increased seizure susceptibility in adult mice
73 recapitulating many features of mTORopathies [16]. However, in order to investigate the
74 function of DEPDC5 during neurodevelopment, new animal models more conducive to the study
75 of early development are required, and hence, we used zebrafish as a handy neurodevelopmental
76 model.

77 In this study, we report the generation and use of a zebrafish model of DEPDC5 loss-of-
78 function to understand the underlying pathological mechanisms. This *depdc5* knockout model
79 showed mTOR hyperactivation, behavioral hypoactivity, spontaneous epileptiform brain events,
80 increased drug-induced seizure susceptibility and premature death. An unbiased transcriptomic
81 analysis of the brains of *depdc5*^{-/-} larvae was performed which showed that, apart from the
82 metabolic perturbation occurring due to mTOR hyperactivation, the regulation of
83 neurodevelopmental pathways was also affected. In particular, fine branching of the GABA
84 network was specifically affected by DEPDC5 knockout. Consistently, treatment with GABA
85 could compensate for some of the defects. Further, these neurodevelopmental changes as well as
86 the transcriptomic changes induced by DEPDC5 knockout occur independently of mTOR
87 signaling. As a result, this study presents new evidence that DEPDC5 is not only involved in
88 mTOR-dependent pathways but is also involved in previously unknown mTOR-independent
89 functions especially during neurodevelopment, a combination of which result in focal epilepsies.

90 These novel insights into the function of DEPDC5 in brain development bring the first evidence
91 of how DEPDC5 loss-of-function could lead to epilepsy.

92

93 **Results:**

94

95 **Depdc5 is essential for vertebrate survival**

96 Though *DEPDC5* mutations were associated with epilepsy, the underlying pathology of
97 this class of focal epilepsies remains unstudied. Zebrafish has only one ortholog of DEPDC5,
98 and sequence alignment of the zebrafish and human proteins showed a high degree of
99 conservation with 75% identity and 84% similarity. Whole mount RNA *in situ* hybridization
100 showed that *depdc5* is expressed in the forebrain, midbrain, hindbrain and also in the neural tube
101 and notochord during zebrafish development (Figure 1A).

102 Using CRISPR/Cas9 genome editing, the 14th exon of *depdc5* encoding the DUF3608,
103 which was initially found to be mutated in many patients [2, 17], was targeted for disruption. A
104 positive founder transmitting a 4-nucleotide frame-shifting deletion was selected, which would
105 lead to the expression a truncated protein (352 amino acids instead of the 1568 residue wild-type
106 protein, Figure 1B). Quantification of mRNA expression showed significant reduction in
107 heterozygous and homozygous larvae (Figure 1C). Since crosses of heterozygotes never resulted
108 in viable juvenile/adult homozygotes, according to the 1:2:1 Mendelian ratio, the survival of all
109 the three genotypes: *depdc5*^{+/+} (wild type), *depdc5*^{+/-} and *depdc5*^{-/-} was monitored for a
110 month from 0 day post fertilization (dpf). While most of the *depdc5*^{+/+} and *+/-* larvae survived
111 for this period, all the *depdc5*^{-/-} larvae died by two weeks of age (Figure 1D). Notably, the
112 survival of *depdc5*^{-/-} can be extended by few days if they are separated early and raised with
113 extra care, although they never survive after 20 dpf. However, no obvious morphological defects

114 or changes in eye size were observed, though a small reduction in body length was seen
115 following quantification (Figures 1E and 1F). While this observation is consistent with the
116 premature death of rodent *Depdc5*^{-/-} models [14-16], the growth delay observed in the complete
117 knockout rodent embryos was not evident in case of *depdc5*^{-/-} zebrafish larvae. Hence, though
118 vertebrates can survive haploinsufficiency of DEPDC5, total absence leads to death during
119 development.

120

121 ***depdc5*^{-/-} larvae show mTOR hyperactivation, brain epileptic discharges, hypoactivity and**
122 **increased seizure susceptibility**

123 Since DEPDC5 is known to negatively regulate mTOR, mTORC1 activity was assessed
124 through the phosphorylation state of the ribosomal protein S6, which is a downstream effector of
125 mTORC1 [18]. Lysates of 8 dpf *depdc5*^{+/+}, *depdc5*^{+/-} and *depdc5*^{-/-} larvae were analyzed by
126 western blotting using antibodies against the S6 Ser240/244 phospho-epitope, and a gradual
127 increase in the phosphorylation was observed (Figure 2A), indicating high mTORC1 activity in
128 the absence of DEPDC5. This was confirmed by performing immunohistological analysis where
129 *depdc5*^{-/-} larval brains showed greater levels of phospho-S6 (Figure 2B). However, no abnormal
130 or dysmorphic cells were visible. In order to monitor epileptic activity, brain activity was
131 monitored using non-invasive local field potential (LFP) recordings from the optic tectum [19].
132 Recurrent spontaneous epileptiform events were observed in *depdc5*^{-/-} larval brains at 9 dpf
133 (Figures 2C and 2D) at a mean frequency of 9.1 ± 5.0 events/10 minutes and mean duration of
134 309.7 ± 152.3 msec, confirming the pathogenicity of DEPDC5 loss-of-function. However, since
135 the LFPs were monitored only for 10 minutes, this epileptic brain activity was observed in only
136 9/42 larvae, and it is possible that many larvae show epileptiform discharges outside this period.
137 Nevertheless, no such events were recorded in different batches of *depdc5*^{+/+} (0 out of 40

138 larvae). It is also possible that these epileptiform discharges manifest earlier but were only
139 monitored at 9 dpf in order to increase the chances of detecting them. The absence of
140 epileptiform discharges in 100% of the animals is consistent with similar observations in *Depdc5*
141 conditional knockout mice and patients with focal epilepsy [16]. In order to have a more accurate
142 readout of the abnormalities in *depdc5*^{-/-} larvae, their locomotor activity was quantified in light-
143 dark cycles. *depdc5*^{-/-} larvae were significantly hypoactive (Figure 2E), and this was observed in
144 100% of the larvae across generations from 5 dpf onward (N>5; n>300), till before death. These
145 results are also consistent with other mTORopathy zebrafish models which show epileptic brain
146 activity and are hypoactive [20]. Interestingly, when coiling (rotating movement of embryo
147 inside the chorion) was monitored at 20 hpf, this earliest motor behavior was already lower in
148 *depdc5*^{-/-} embryos (Figure 2F), indicating that the hypoactivity begins very early during
149 development, suggesting that DEPDC5 loss-of-function may have consequences on early
150 neurodevelopment. Lastly, the susceptibility of *depdc5*^{-/-} larvae to chemically-induced seizures
151 by pentylenetetrazol (PTZ) was tested. Consistently with what have been reported in mice [16],
152 *depdc5*^{-/-} larvae show a significantly increased response to PTZ (shorter delay of response to
153 PTZ exposure and higher swimming activity) compared to their siblings (Figure 2G and 2H).

154 Altogether, the phenotypes observed upon knocking out *depdc5* in zebrafish are
155 reminiscent of what is observed in the existing rodent models of *Depdc5* knockout and also to an
156 extent, in patients. Altogether, these results validate the pathogenicity of *depdc5* loss-of-function
157 in zebrafish.

158

159 **Alteration of brain gene expression profile in *depdc5*^{-/-}**

160 In order to obtain new unbiased insights into the molecular perturbations occurring
161 during neurodevelopment in the absence of DEPDC5, brains of 10 dpf *depdc5*^{+/+} and *-/-* larvae
162 were dissected out and total RNA was extracted for deep sequencing (Figure 3A). This age was
163 chosen as an intermediate stage to perform exhaustive analysis of the molecular phenotype at a
164 stage when the swimming phenotype is distinct, while preventing the perturbation of gene
165 expression by the premature death that occurs 5 days later. From the differential gene expression
166 analysis, 1191 genes out of approximately 12,000 genes expressed in the larval brain were found
167 to be significantly up- (532 genes) or downregulated (659 genes) ($p < 0.05$) (full list can be found
168 in Table S1, description provided for top dysregulated genes). Notably, 16 out of the 20
169 aminoacyl-tRNA synthetases in zebrafish were upregulated in the *depdc5*^{-/-} brains, presumably
170 due to improper mTOR regulation. Functional annotation and clustering of the significantly
171 dysregulated genes showed that apart from aminoacyl-tRNA biosynthesis and electron transport
172 chain that can be attributed to mTOR pathway dysfunction, the expression of genes involved in
173 other pathways including chordate embryonic pattern specification, regulation of neuron
174 projection morphogenesis/axonogenesis, synapse formation, zinc finger/transcription factors and
175 ion channels were also perturbed (Figure 3B). This suggested that DEPDC5 may also play a role
176 in embryonic neurodevelopment.

177 Since genes related to neurodevelopment were altered, the number of neurons during
178 developmental stages was analyzed. Measurement of the head size and staining with cresyl violet
179 showed that the size and morphology of *depdc5*^{-/-} larval brains were similar to that of the control
180 (Figures 3D and 3F). In addition, using immunostaining against acetylated tubulin and
181 phosphorylated histone H3 (which label neuronal fibres and mitotic cells respectively), the main
182 brain networks and neurogenesis itself did not appear to be affected (Figures 3C and 3E).

183 However, many genes related to GABAergic networks which have conventionally been
184 correlated with other kinds of epilepsy, were downregulated. Indeed, 3 GABA receptors
185 (GABRA1, GABBR1b and GABRG2) and other associated factors required for synthesis and
186 transport of GABA, GABAergic synapse formation, maturation and transmission (like Gat3,
187 pyruvate carboxylase, Kcc2 and neuroligin 2) were all downregulated (Table S3).

188 Since the expression of multiple factors important for GABAergic network formation and
189 synaptic function was perturbed, the expression of three markers of inhibitory synapses,
190 Gad65/67, gephyrin and neuroligin-2 (Nlgn-2), was examined by immunostaining of transverse
191 sections from 8 dpf *depdc5*^{+/+} and *depdc5*^{-/-} larval brains. Interestingly, close examination of
192 the sections immunostained with Gad65/67 showed that finer branched structures were not
193 present as in wild type siblings (Figure 4A). 3D reconstruction of Gad65/67 staining confirmed
194 that the Gad65/67 projections (in blue in Figure 4B) are less arborized in the mutant brains.
195 Since GABA synthesizing enzymes are expressed in clusters at the pre-synaptic GABA synapses,
196 these results confirm defects in the GABAergic network connectivity. Immunolabeling against
197 gephyrin and Nlgn2 also showed a significant decrease of the complexity in *depdc5*^{-/-} brains
198 (Figures 4C and 4D). Upon quantifying the GAD65/67 and gephyrin positive neurofilaments and
199 puncta from at least three biological replicates, both were decreased by >50% in *depdc5*^{-/-}
200 (Figure 4F). Lastly, immunolabelling and quantification of the interneuron population using
201 parvalbumin 7 antibody did not show any difference in the number of positive cells (Figure 4E
202 and 4F). These results demonstrate that DEPDC5 loss-of-function significantly impacts fine
203 branching of GABAergic network during neurodevelopment without causing major loss of
204 interneurons.

205

206 **GABA exposure rescues hypoactivity and seizure susceptibility in *depdc5*^{-/-} larvae through**
207 **paracrine effects**

208 Since the expression of GABA synthesizing enzymes seemed to be affected, we
209 hypothesized that exposure to GABA may compensate for this decrease and could therefore
210 rescue the consistent hypoactivity and seizure susceptibility phenotypes of *depdc5*^{-/-} larvae.
211 Concurrently with this hypothesis, GABA treatment could completely rescue the hypoactivity of
212 *depdc5*^{-/-} larvae (swimming at 7 dpf and coiling at 24 hpf) (Figures 5A and 5B). Rapamycin,
213 which has a positive effect on other mTORopathy models, was used as a positive control, and
214 could also completely rescue the hypoactivity of *depdc5*^{-/-} embryos and the increased phospho-
215 S6 levels (Figures 5A-C). Moreover, GABA treatment, as well as rapamycin could rescue the
216 seizure susceptibility of *depdc5*^{-/-} larvae exposed to PTZ, to the level of their siblings (Figures
217 5D and 5E). Hence, these results confirm earlier observations from transcriptomic and
218 immunolabelling experiments that GABA network/signalling is indeed altered in *depdc5*^{-/-}
219 larvae. Moreover, it shows that both GABA and mTOR signalling are involved in the
220 pathogenicity of *depdc5* loss-of-function.

221 In order to assess if this rescuing effect could be a result of a rescue of the
222 neurodevelopmental defects themselves, neuronal branching of GABAergic neurons was
223 monitored following GABA treatment. However, supplementation with GABA could not rescue
224 the fine neuronal branching defects observed in *depdc5*^{-/-} larvae (Figures 5F and 5G) thus
225 suggesting that GABA can only *compensate for*, but *not rescue* the neurodevelopmental defects.
226 Further, when the effect of GABA and rapamycin treatment on larval survival was tested, GABA
227 exposure could not rescue the premature death at 2-3 weeks post fertilization (wpf), while
228 rapamycin treatment extended the life span as long as it was supplemented (Figure 5H). This

229 supports our conclusion that GABA exposure can only partially compensate for the
230 neurodevelopmental defects.

231 Hence, these results show that while increasing GABA levels could compensate for
232 defective GABAergic branching, it could not rescue the neurodevelopmental defect itself. This
233 also indicates that the premature death is essentially due to perturbation of mTOR signaling
234 (which could be rescued by rapamycin), rather than the GABA network defects. Indeed,
235 rapamycin needed to be continually supplemented, since withdrawal of rapamycin led to gradual
236 death (Figure 5H), reiterating the contribution of mTOR deregulation to premature death.

237 In order to understand if the compensating effect of GABA was mediated through GABA
238 receptors or independently of them, muscimol (a GABA_A receptor agonist), baclofen (a GABA_B
239 receptor agonist) and vigabatrin (an inhibitor of GABA transaminase which increases local
240 GABA concentration) were tested for their effect on *depdc5*^{-/-} larvae (Figure 6A). Interestingly,
241 treatment with the GABA receptor agonists, muscimol, baclofen, and even both in combination
242 could not rescue the hypoactivity. However, exposure to vigabatrin, which increases endogenous
243 GABA level by inhibiting its metabolism, completely rescued the hypoactivity of *depdc5*^{-/-}
244 larvae as well as PTZ hypersensitivity (Figure 6B). This proves that GABA acts through
245 receptor-independent mechanisms in a paracrine fashion. Moreover, the fact that inhibiting
246 GABA metabolism using vigabatrin is sufficient to rescue the phenotype suggests that GABA
247 itself mediates the compensating effects rather than metabolites of GABA.

248 Altogether these results support the idea that DEPDC5 loss-of-function impairs early
249 neurodevelopment especially GABA network fine branching which is likely to contribute to
250 epileptogenesis, and that mTOR-dependent metabolic changes are more generalized and severe,
251 eventually resulting in premature death.

252

253 **mTOR-dependent and independent pathways are perturbed in *depdc5*^{-/-} larvae**

254 In order to further understand whether these two phenomena: upregulation of mTOR
255 signaling, and defective development of GABAergic networks are related and act together in the
256 same pathway, or are controlled independently by DEPDC5, the *depdc5*^{-/-} differentially
257 expressed gene dataset was compared to datasets from three other zebrafish models of epilepsy.
258 These included: (1) a *gabral*^{-/-} zebrafish line recapitulating idiopathic generalized epilepsy, in
259 which GABAergic network is defective (Samarut et al., under review) (2) an mTORopathy
260 epilepsy (*tsc2*^{-/-}) zebrafish model in which mTORC1 activity is increased [20], and (3) a Dravet
261 syndrome zebrafish model (*scn1Lab* mutant carrying a mutation in Nav1.1 [21]), as a neutral
262 mTOR- and GABA-non-related epilepsy model (Figure 6C).

263 177 genes were found to overlap between the *depdc5* and *gabral* datasets (15% and 40%
264 of the total number of genes in the *depdc5* and *gabral* datasets respectively), and remarkably,
265 99% of them (175/177) showed the same trend of up- or downregulation in both datasets
266 suggesting specific common mechanisms. When functional clustering and annotation of the
267 common genes was performed, these genes were found to be involved in electron transport,
268 embryonic morphogenesis, GABA receptor activity, synapse formation, general synaptic
269 activity, axonogenesis, nucleotide binding and transcription (Figure 6D and Table S3).
270 Interestingly, many factors which have been associated with epilepsy earlier were also
271 dysregulated. This significant overlap between *depdc5* and *gabral* datasets provides further
272 evidence that DEPDC5 loss-of-function induces broad defects in GABA network.

273 Since both DEPDC5 and TSC2 are involved in the negative regulation of mTOR,
274 common genes between these two datasets showed mTOR-related pathways as the largest group

275 of genes, upon functional clustering and annotation (Table S4). About 15% genes of the two
276 datasets were found to be genes encoding for mTOR related members like aminoacyl-tRNA
277 synthetases, stress response and protein phosphorylation. The overlap of the *depdc5* dataset with
278 data from other models of epilepsy (*Scn1Lab*) and autism spectrum disorder (unpublished, data
279 not shown) did not show a significant overlap (only 23 genes in common between *depdc5*^{-/-} and
280 *Scn1Lab*^{-/-} datasets) thus confirming the specificity of the overlaps described above.

281 Surprisingly, among the 177 common genes between the *gabral* and *depdc5* datasets
282 which were involved in neurogenesis and GABA networks, only 18 genes were found to be
283 common with the *tsc2* dataset. The non-overlapping nature of 90% (159 of 177) of the genes
284 indicates that these neurodevelopment-associated genes are more likely to be unrelated to
285 mTOR, but rather controlled by DEPDC5 independently of its canonical mTOR-inhibitory
286 function. These observations show that in the absence of DEPDC5, there are mTOR-dependent
287 metabolic changes (which overlap with the *tsc2* model) but also mTOR-independent
288 neurodevelopment defects especially in the GABAergic network (which overlap with the *gabral*
289 model), a combination of which presumably leads to epilepsy.

290

291 **Neurodevelopmental defects in *depdc5*^{-/-} larvae are independent of mTOR signaling**

292 In order to confirm the independent nature of the mTOR and GABA pathways, mTOR
293 signaling was assessed following treatment with GABA in *depdc5*^{+/+} and ^{-/-} larvae (Figure
294 7A). Consistent with the hypothesis, GABA treatment could not rescue the increase in mTOR
295 activity in *depdc5*^{-/-} larvae (Figure 7A, upper panel). Moreover, the levels of phospho-S6 were
296 also checked in *gabral*^{-/-} larvae, which have defective GABA signaling and it did not show any

297 change (Figure 7A lower panel). These results indicate that GABA and its related metabolism do
298 not control mTOR signaling.

299 Further, in order to confirm that the neurodevelopmental defects induced by *depdc5* loss-
300 of-function are indeed mTOR-independent, the ability of rapamycin to rescue the fine branching
301 of the GABAergic network in *depdc5*^{-/-} larval brains was assessed. Brain slices from rapamycin
302 treated *depdc5*^{+/+} and ^{-/-} larvae were immunostained using α -GAD65/67. Rapamycin treatment
303 failed to rescue the reduced fine branching of the GABAergic network during development in
304 *depdc5*^{-/-}. Indeed, similar to what was observed in untreated *depdc5*^{-/-} brains (Figure 4), the
305 GAD65/67-positive neurofilaments were less arborized even after rapamycin treatment (Figure
306 7B and 7C), proving that the GABAergic branching defects resulting from the absence of
307 DEPDC5 are indeed mTOR-independent. Of note, phospho-S6 levels are significantly reduced
308 when rapamycin was applied at this concentration (Figure 7D).

309 To confirm the mTOR-independent effects at the molecular level, the ability of
310 rapamycin to restore the expression of critical up- and downregulated genes back to normal was
311 tested in order to assess if the transcriptional changes were also mTOR independent. The genes
312 that were chosen for testing by RT-qPCR were related to axon guidance (*plx2a*, *sema3b*,
313 *efnb3b*) and GABA synapse (*gabrg2*, *gat3*, *kcc2*), which were in common with the *gabral*
314 dataset, and also some mitochondrial factors (*mt-cyb*, *mt-co2*). Consistently with their
315 involvement in metabolic processes, the expression of mitochondrial cytochrome B and
316 cytochrome C oxidase II genes in *depdc5*^{-/-} brains was decreased to wild-type level upon
317 rapamycin treatment (Figure 7E). However, for the genes involved in axon guidance and GABA
318 synapse activity, rapamycin treatment could not rescue the reduced expression observed in
319 *depdc5*^{-/-} larval brains (Figure 7E). This incapability of rapamycin to rescue both, the

320 neurodevelopmental defects and the transcriptional changes proves that the molecular defects are
321 indeed mTOR-independent.

322 Lastly, if GABAergic network defects induced by *DEPDC5* knockout are mTOR
323 independent, GABA would not have any effect on another genetic model of mTOR
324 hyperactivation such as *tsc2*^{-/-} [20]. Consistently, when tested on *tsc2*^{-/-} larvae, GABA was
325 unable to rescue the hypoactivity, again validating the mTOR-independent nature of the defects
326 observed in *depdc5*^{-/-} larvae (Figure 7F). Of note, rapamycin, which was used as a positive
327 control could rescue the hypoactivity observed in *tsc2*^{-/-} larvae.

328 Hence, these results show that at the phenotypic, cellular and molecular levels, alongside
329 its canonical mTOR inhibitory function, DEPDC5 does control neurodevelopmental aspects of
330 GABAergic networks in an mTOR independent fashion.

331

332 **Discussion:**

333 Mutations in the members of the mTOR-inhibitory GATOR1 complex have recently been
334 shown to be associated with focal epilepsy [7-10]. However, multiple aspects of this complex
335 remain poorly understood, including the molecular pathways through which it plays a role in
336 normal brain activity and/or development.

337 *Depdc5* is strongly expressed in the developing vertebrate nervous system as shown by *in*
338 *situ* hybridization of early zebrafish embryos, indicating a role for this protein in neuronal
339 development. DEPDC5 is expressed specifically in neurons in the human brain (Human protein
340 atlas database and Human brain transcriptome project) where the transcript was first identified
341 [2, 22], but this is the first report showing its strong expression in the developing vertebrate
342 neural system.

343 In order to understand the role of DEPDC5 in neurodevelopment and brain activity, the
344 first zebrafish knockout model of *depdc5* was generated and studied. Although rodent models
345 have been recently generated [14-16], the zebrafish model proffers specific technical advantages
346 for studying early neurodevelopment. Though *depdc5*^{-/-} zebrafish larvae do not show obvious
347 phenotypic changes, they exhibit transient spontaneous epileptiform discharges in their brain and
348 increased seizure susceptibility before they die prematurely at about 2 wpf. The zebrafish model
349 also proffers a platform for drug screening purposes. Our zebrafish model would be convenient
350 for initial high-throughput drug screening assays that could identify candidate molecules
351 restoring *depdc5*^{-/-} larval phenotype (i.e. hypoactivity and seizure susceptibility) and later be
352 confirmed in mammalian models. Such an approach using complementary vertebrate models has
353 proven to be effective and time-saving in identifying new therapeutics for other genetic diseases
354 [23].

355 Hypoactivity and seizure susceptibility of the larvae was consistently observed and could
356 be used as an accurate readout for further studies. It is noteworthy that another zebrafish model
357 with hyperactive mTOR owing to mutated *tsc2* also shows hypoactivity and premature death
358 along with epileptic seizures [20]. Also, since the hypoactivity is observed from very early on,
359 coiling could also be used as a readout in drug screening to economize on time. Notably, no
360 enlarged or abnormal cells were detected in the developing zebrafish brains in this model. This
361 could be explained by the “two-hit” hypothesis where an additional hit along with *DEPDC5*
362 mutations occurs to cause FCD in patients [9]. Also, though *depdc5*^{-/-} larvae show considerably
363 less mRNA levels, it was not completely absent, probably due to incomplete degradation of
364 *depdc5* mRNA by nonsense-mediated decay. However, the significant reduction of mRNA levels
365 show that the phenotypes observed were a result of haploinsufficiency.

366 With the aim to get further insights into the molecular perturbations in the epileptic
367 *depdc5*^{-/-} brains, transcriptomic analysis was performed in this study, which showed interesting
368 candidates that were up- or downregulated. This is the first report of an *in vivo* transcriptomic
369 profile from a model of dysfunctional GATOR1 complex. As expected, various mTOR-regulated
370 pathways like amino acid metabolism were upregulated owing to mTOR deregulation, including
371 most amino acyl tRNA synthetases. While loss-of-function mutations in some aminoacyl-tRNA
372 synthetases have been shown to be associated with epilepsy [24-27], the contribution of such a
373 broad upregulation in expression levels of these factors to epilepsy remains to be understood.

374 Interestingly, though factors associated with neurogenesis, axonogenesis and synaptic
375 functions were downregulated, rather than gross morphological defect or neuron loss, specific
376 downregulation of GABA receptors, transporters and factors involved in inhibitory network
377 development, synapse formation and function was observed, revealing for the first time the
378 possible role of DEPDC5 in the formation, pruning and maintenance of the GABAergic system.

379 GABA exposure could partially compensate the phenotype observed in *depdc5*^{-/-} larvae.
380 The use of GABA receptor agonists in mTORopathies has been explored only for TSC [28], but
381 muscimol and baclofen were ineffective in *depdc5*^{-/-} larvae. These observations suggest that the
382 compensating effect of GABA is more likely to be a paracrine effect of GABA rather than
383 through GABA receptors. In this context, the ability of vigabatrin to rescue the phenotype also
384 confirms the direct effect of GABA rather than of its metabolites. Notably, GABA can only
385 partially ameliorate the *depdc5*^{-/-} phenotype and therefore cannot be considered as a candidate
386 drug against refractory epilepsies. However, the observation that GABAergic networks are
387 affected early during development in a vertebrate *DEPDC5* knockout model is an important
388 consideration for treatment strategies. Indeed, it might be useful to design therapeutic strategies

389 that can restore or at least compensate stably, the neurodevelopmental defects, rather than solely
390 trying to treat symptomatically, i.e., alleviate the seizures. Notably, the paracrine effect of
391 GABA observed here is also significant since many patients with mutations in *DEPDC5* are
392 refractory to conventional anti-epileptic drugs, which generally act through GABA receptors
393 such as benzodiazepines. Thus, the application of molecules that would increase GABA
394 signaling independently of GABA receptors (such as vigabatrin) could be interesting in the
395 context of these refractory epilepsies.

396 Predictably, rapamycin could rescue the phenotype, and also prevent premature death,
397 suggesting that mTOR deregulation affects multiple organismal functions. Rapamycin and
398 rapalogs have proved to be extremely effective against many mTOR associated diseases
399 including cancer, lymphangiomyomatosis (LAM) and tuberous sclerosis [29-31]. Rapamycin
400 has also been shown to extend longevity and have neuroprotective effects [32, 33]. Like in
401 earlier studies with other diseases, though very effective, cessation of rapamycin treatment led to
402 reappearance of the symptoms and death [30, 34]. Due to various reasons including activation of
403 alternate or compensatory pathways, rapamycin treatment has had modest outcomes in clinical
404 trials despite very promising pre-clinical animal model studies [35]. Hence, rapamycin and
405 rapalogs are now being tested for combination therapy as chemotherapeutic agents, and these
406 could also be applied to treat focal epilepsies, since there is a need to identify new targetable
407 mechanisms of focal epilepsy in order to design new drugs against refractory seizures.

408 Through multiple comparison of transcriptomic datasets, a large set of genes from the
409 *depdc5* dataset was found to overlap with the *gabral* dataset independently of the *tsc2* dataset,
410 suggesting that DEPDC5 has unexpected mTOR-independent activity, especially in regulating
411 GABA network development, as proven experimentally (Figure 7). Hence, it is possible that the

412 two inhibitory complexes, GATOR1 (via DEPDC5) and TSC play distinct roles in different
413 pathways and cell types in addition to their overlapping mTOR-related functions. DEPDC5
414 function is still incompletely understood and many epileptic mutations have been identified in
415 different domains of DEPDC5 including DUF3608 [2, 3], which also supports the idea that there
416 could be other yet undiscovered functions of DEPDC5. Though mTOR activity has been
417 associated with proper neuronal development [36-38], this study shows that the
418 neurodevelopmental role of DEPDC5 is mTOR-independent. Hence, in addition to controlling
419 neuronal development through mTOR, the components of the pathway might also have mTOR-
420 independent roles.

421 Altogether, these results show a novel mTOR-independent effect of DEPDC5 on the
422 GABAergic network that is very likely to be a key component of DEPDC5-mediated focal
423 epilepsy substratum. Indeed, abnormal wiring and functioning of the GABAergic system have
424 been observed in epilepsy [39] and GABA agonists have been used for decades alongside other
425 drugs like sodium and calcium channel blockers, glutamate blockers, carbonic anhydrase
426 inhibitors, and other drugs as anti-epileptics [40, 41]. Since GABA is the primary inhibitory
427 neurotransmitter in the cortex, GABA agonists have long been considered the logical choice as
428 anti-epileptic agents. However, in the emerging field of epilepsies caused by mutations in non-
429 ion channel genes, the contribution of the GABAergic network to epilepsy has not been studied
430 and this study shows that modulation of the GABAergic network together with targeting mTOR
431 could be very effective against this class of non-ion channelopathies.

432

433 **Acknowledgements:**

434 We thank Dr. Louis-Charles Levros and Prof. Patrick Cossette for useful discussions regarding
435 the GABA agonists, Florent Guilloteau and Patrick Gendron from the IRIC genomic platform for
436 discussions regarding the RNA-sequencing experiment, Marina Drits for assistance with fish
437 maintenance. We thank Dr. Kessen Patten and Prof. Jacques Samarut for critical reading and
438 valuable comments on the manuscript. This work was funded by The Savoy Foundation, the
439 Fonds de Recherche Québec Santé (FRQS), the Rare Disease Model and Mechanism network,
440 Dravet Canada, FRQS-affiliated GRSNC (Groupe de Recherche sur le Système Nerveux
441 Central), the Québec MEESR (Ministère de l'Éducation, de l'Enseignement Supérieur et de
442 Recherche), the CRCHUM and the Agence Nationale pour la Recherche (ANR) (grant ANR-16-
443 CE18-0010 to N.S.Y.).

444

445 **Author contributions:**

446 The project was conceptualized by ES and PD. ES generated and characterized the CRISPR line
447 with assistance from ML and RR. AS and ES performed most of the experiments. AIS and
448 PAMW performed the analyzed the brain epileptiform activity. NSY designed and analyzed the
449 immunolabeling experiment, which RHA and SR performed. AS and ES wrote the manuscript,
450 which was edited by PD.

451

452 **Declaration of interests:** The authors declare no competing interests.

453

454 **References:**

- 455 1. Baulac, S. (2014). Genetics advances in autosomal dominant focal epilepsies: focus on
456 DEPDC5. *Prog Brain Res* 213, 123-139.

- 457 2. Dibbens, L.M., de Vries, B., Donatello, S., Heron, S.E., Hodgson, B.L., Chintawar, S.,
458 Crompton, D.E., Hughes, J.N., Bellows, S.T., Klein, K.M., et al. (2013). Mutations in
459 DEPDC5 cause familial focal epilepsy with variable foci. *Nat Genet* 45, 546-551.
- 460 3. Ishida, S., Picard, F., Rudolf, G., Noe, E., Achaz, G., Thomas, P., Genton, P., Mundwiler,
461 E., Wolff, M., Marescaux, C., et al. (2013). Mutations of DEPDC5 cause autosomal
462 dominant focal epilepsies. *Nat Genet* 45, 552-555.
- 463 4. Xiong, L., Labuda, M., Li, D.S., Hudson, T.J., Desbiens, R., Patry, G., Verret, S., Langevin,
464 P., Mercho, S., Seni, M.H., et al. (1999). Mapping of a gene determining familial partial
465 epilepsy with variable foci to chromosome 22q11-q12. *Am J Hum Genet* 65, 1698-1710.
- 466 5. Picard, F., Makrythanasis, P., Navarro, V., Ishida, S., de Bellescize, J., Ville, D.,
467 Weckhuysen, S., Fosselle, E., Suls, A., De Jonghe, P., et al. (2014). DEPDC5 mutations in
468 families presenting as autosomal dominant nocturnal frontal lobe epilepsy. *Neurology*
469 82, 2101-2106.
- 470 6. Bar-Peled, L., Chantranupong, L., Cherniack, A.D., Chen, W.W., Ottina, K.A., Grabiner,
471 B.C., Spear, E.D., Carter, S.L., Meyerson, M., and Sabatini, D.M. (2013). A Tumor
472 suppressor complex with GAP activity for the Rag GTPases that signal amino acid
473 sufficiency to mTORC1. *Science* 340, 1100-1106.
- 474 7. Ricos, M.G., Hodgson, B.L., Pippucci, T., Saidin, A., Ong, Y.S., Heron, S.E., Licchetta, L.,
475 Bisulli, F., Bayly, M.A., Hughes, J., et al. (2016). Mutations in the mammalian target of
476 rapamycin pathway regulators NPRL2 and NPRL3 cause focal epilepsy. *Ann Neurol* 79,
477 120-131.
- 478 8. Scheffer, I.E., Heron, S.E., Regan, B.M., Mandelstam, S., Crompton, D.E., Hodgson, B.L.,
479 Licchetta, L., Provini, F., Bisulli, F., Vadlamudi, L., et al. (2014). Mutations in mammalian
480 target of rapamycin regulator DEPDC5 cause focal epilepsy with brain malformations.
481 *Ann Neurol* 75, 782-787.
- 482 9. Baulac, S., Ishida, S., Marsan, E., Miquel, C., Biraben, A., Nguyen, D.K., Nordli, D.,
483 Cossette, P., Nguyen, S., Lambrecq, V., et al. (2015). Familial focal epilepsy with focal
484 cortical dysplasia due to DEPDC5 mutations. *Ann Neurol* 77, 675-683.
- 485 10. D'Gama, A.M., Geng, Y., Couto, J.A., Martin, B., Boyle, E.A., LaCoursiere, C.M., Hossain,
486 A., Hatem, N.E., Barry, B.J., Kwiatkowski, D.J., et al. (2015). Mammalian target of
487 rapamycin pathway mutations cause hemimegalencephaly and focal cortical dysplasia.
488 *Ann Neurol* 77, 720-725.
- 489 11. Crino, P.B. (2016). The mTOR signalling cascade: paving new roads to cure neurological
490 disease. *Nat Rev Neurol* 12, 379-392.
- 491 12. Ostendorf, A.P., and Wong, M. (2015). mTOR inhibition in epilepsy: rationale and clinical
492 perspectives. *CNS Drugs* 29, 91-99.
- 493 13. Palavra, F., Robalo, C., and Reis, F. (2017). Recent Advances and Challenges of mTOR
494 Inhibitors Use in the Treatment of Patients with Tuberous Sclerosis Complex. *Oxid Med*
495 *Cell Longev* 2017, 9820181.
- 496 14. Marsan, E., Ishida, S., Schramm, A., Weckhuysen, S., Muraca, G., Lecas, S., Liang, N.,
497 Treins, C., Pende, M., Roussel, D., et al. (2016). Depdc5 knockout rat: A novel model of
498 mTORopathy. *Neurobiol Dis* 89, 180-189.
- 499 15. Hughes, J., Dawson, R., Tea, M., McAninch, D., Piltz, S., Jackson, D., Stewart, L., Ricos,
500 M.G., Dibbens, L.M., Harvey, N.L., et al. (2017). Knockout of the epilepsy gene Depdc5 in

501 mice causes severe embryonic dysmorphology with hyperactivity of mTORC1 signalling.
502 Sci Rep 7, 12618.

503 16. Yuskaitis, C.J., Jones, B.M., Wolfson, R.L., Super, C.E., Dhamne, S.C., Rotenberg, A.,
504 Sabatini, D.M., Sahin, M., and Poduri, A. (2017). A mouse model of DEPDC5-related
505 epilepsy: Neuronal loss of Depdc5 causes dysplastic and ectopic neurons, increased
506 mTOR signaling, and seizure susceptibility. *Neurobiol Dis* 111, 91-101.

507 17. Martin, C., Meloche, C., Rioux, M.F., Nguyen, D.K., Carmant, L., Andermann, E., Gravel,
508 M., and Cossette, P. (2014). A recurrent mutation in DEPDC5 predisposes to focal
509 epilepsies in the French-Canadian population. *Clin Genet* 86, 570-574.

510 18. Hay, N., and Sonenberg, N. (2004). Upstream and downstream of mTOR. *Genes Dev* 18,
511 1926-1945.

512 19. Zdebik, A.A., Mahmood, F., Stanescu, H.C., Kleta, R., Bockenbauer, D., and Russell, C.
513 (2013). Epilepsy in *kcnj10* morphant zebrafish assessed with a novel method for long-
514 term EEG recordings. *PLoS One* 8, e79765.

515 20. Scheldeman, C., Mills, J.D., Siekierska, A., Serra, I., Copmans, D., Iyer, A.M., Whalley, B.J.,
516 Maes, J., Jansen, A.C., Lagae, L., et al. (2017). mTOR-related neuropathology in mutant
517 *tsc2* zebrafish: Phenotypic, transcriptomic and pharmacological analysis. *Neurobiol Dis*
518 108, 225-237.

519 21. Baraban, S.C., Dinday, M.T., and Hortopan, G.A. (2013). Drug screening in *Scn1a*
520 zebrafish mutant identifies clemizole as a potential Dravet syndrome treatment. *Nat*
521 *Commun* 4, 2410.

522 22. Ishikawa, K., Nagase, T., Suyama, M., Miyajima, N., Tanaka, A., Kotani, H., Nomura, N.,
523 and Ohara, O. (1998). Prediction of the coding sequences of unidentified human genes.
524 X. The complete sequences of 100 new cDNA clones from brain which can code for large
525 proteins in vitro. *DNA Res* 5, 169-176.

526 23. Patten, S.A., Aggad, D., Martinez, J., Tremblay, E., Petrillo, J., Armstrong, G.A., La
527 Fontaine, A., Maios, C., Liao, M., Ciura, S., et al. (2017). Neuroleptics as therapeutic
528 compounds stabilizing neuromuscular transmission in amyotrophic lateral sclerosis. *JCI*
529 *Insight* 2.

530 24. Almalki, A., Alston, C.L., Parker, A., Simonic, I., Mehta, S.G., He, L., Reza, M., Oliveira,
531 J.M., Lightowlers, R.N., McFarland, R., et al. (2014). Mutation of the human
532 mitochondrial phenylalanine-tRNA synthetase causes infantile-onset epilepsy and
533 cytochrome c oxidase deficiency. *Biochim Biophys Acta* 1842, 56-64.

534 25. Zhang, X., Ling, J., Barcia, G., Jing, L., Wu, J., Barry, B.J., Mochida, G.H., Hill, R.S., Weimer,
535 J.M., Stein, Q., et al. (2014). Mutations in QARS, encoding glutamyl-tRNA synthetase,
536 cause progressive microcephaly, cerebral-cerebellar atrophy, and intractable seizures.
537 *Am J Hum Genet* 94, 547-558.

538 26. Hallmann, K., Zsurka, G., Moskau-Hartmann, S., Kirschner, J., Korinthenberg, R., Ruppert,
539 A.K., Ozdemir, O., Weber, Y., Becker, F., Lerche, H., et al. (2014). A homozygous splice-
540 site mutation in CARS2 is associated with progressive myoclonic epilepsy. *Neurology* 83,
541 2183-2187.

542 27. Nishri, D., Goldberg-Stern, H., Noyman, I., Blumkin, L., Kivity, S., Saitsu, H., Nakashima,
543 M., Matsumoto, N., Leshinsky-Silver, E., Lerman-Sagie, T., et al. (2016). RARS2 mutations

544 cause early onset epileptic encephalopathy without ponto-cerebellar hypoplasia. *Eur J*
545 *Paediatr Neurol* *20*, 412-417.

546 28. Curatolo, P., Verdecchia, M., and Bombardieri, R. (2001). Vigabatrin for tuberous
547 sclerosis complex. *Brain Dev* *23*, 649-653.

548 29. Wander, S.A., Hennessy, B.T., and Slingerland, J.M. (2011). Next-generation mTOR
549 inhibitors in clinical oncology: how pathway complexity informs therapeutic strategy. *J*
550 *Clin Invest* *121*, 1231-1241.

551 30. Bissler, J.J., McCormack, F.X., Young, L.R., Elwing, J.M., Chuck, G., Leonard, J.M.,
552 Schmithorst, V.J., Laor, T., Brody, A.S., Bean, J., et al. (2008). Sirolimus for
553 angiomyolipoma in tuberous sclerosis complex or lymphangiomyomatosis. *N Engl J*
554 *Med* *358*, 140-151.

555 31. Muncy, J., Butler, I.J., and Koenig, M.K. (2009). Rapamycin reduces seizure frequency in
556 tuberous sclerosis complex. *J Child Neurol* *24*, 477.

557 32. Bové, J., Martínez-Vicente, M., and Vila, M. (2011). Fighting neurodegeneration with
558 rapamycin: mechanistic insights. *Nat Rev Neurosci* *12*, 437-452.

559 33. Harrison, D.E., Strong, R., Sharp, Z.D., Nelson, J.F., Astle, C.M., Flurkey, K., Nadon, N.L.,
560 Wilkinson, J.E., Frenkel, K., Carter, C.S., et al. (2009). Rapamycin fed late in life extends
561 lifespan in genetically heterogeneous mice. *Nature* *460*, 392-395.

562 34. McCormack, F.X., Inoue, Y., Moss, J., Singer, L.G., Strange, C., Nakata, K., Barker, A.F.,
563 Chapman, J.T., Brantly, M.L., Stocks, J.M., et al. (2011). Efficacy and safety of sirolimus in
564 lymphangiomyomatosis. *N Engl J Med* *364*, 1595-1606.

565 35. Li, J., Kim, S.G., and Blenis, J. (2014). Rapamycin: one drug, many effects. *Cell Metab* *19*,
566 373-379.

567 36. Fu, C., Cawthon, B., Clinkscales, W., Bruce, A., Winzenburger, P., and Ess, K.C. (2012).
568 GABAergic interneuron development and function is modulated by the Tsc1 gene. *Cereb*
569 *Cortex* *22*, 2111-2119.

570 37. Westerholz, S., de Lima, A.D., and Voigt, T. (2013). Thyroid hormone-dependent
571 development of early cortical networks: temporal specificity and the contribution of
572 trkB and mTOR pathways. *Front Cell Neurosci* *7*, 121.

573 38. Garza-Lombó, C., and Gonsebatt, M.E. (2016). Mammalian Target of Rapamycin: Its Role
574 in Early Neural Development and in Adult and Aged Brain Function. *Front Cell Neurosci*
575 *10*, 157.

576 39. Treiman, D.M. (2001). GABAergic mechanisms in epilepsy. *Epilepsia* *42 Suppl 3*, 8-12.

577 40. Ashton, H., and Young, A.H. (2003). GABA-ergic drugs: exit stage left, enter stage right. *J*
578 *Psychopharmacol* *17*, 174-178.

579 41. Jembrek, M.J., and Vlainic, J. (2015). GABA Receptors: Pharmacological Potential and
580 Pitfalls. *Curr Pharm Des* *21*, 4943-4959.

581 42. Moreno-Mateos, M.A., Vejnar, C.E., Beaudoin, J.D., Fernandez, J.P., Mis, E.K., Khokha,
582 M.K., and Giraldez, A.J. (2015). CRISPRscan: designing highly efficient sgRNAs for CRISPR-
583 Cas9 targeting in vivo. *Nat Methods* *12*, 982-988.

584 43. Thisse, C., and Thisse, B. (2008). High-resolution in situ hybridization to whole-mount
585 zebrafish embryos. *Nat Protoc* *3*, 59-69.

- 586 44. Huang da, W., Sherman, B.T., and Lempicki, R.A. (2009). Systematic and integrative
587 analysis of large gene lists using DAVID bioinformatics resources. *Nature Protocols* 4, 44-
588 57.
- 589 45. Puverel, S., Nakatani, H., Parras, C., and Soussi-Yanicostas, N. (2009). Prokineticin
590 receptor 2 expression identifies migrating neuroblasts and their subventricular zone
591 transient-amplifying progenitors in adult mice. *J Comp Neurol* 512, 232-242.

592

593

594 **Figure legends:**

595 **Figure 1: *depdc5* is essential for survival.** (A) Whole mount *in situ* hybridization showing
596 expression of *depdc5* at different stages of development. (B) Electropherograms showing
597 confirmation of the 4 bp insertion by Sanger sequencing. (C) Expression of *depdc5* transcript in
598 7 dpf *depdc5*^{+/+}, *depdc5*^{+/-} and *depdc5*^{-/-} larvae (N=3, Student's t test: p (WT vs HT)=0.0026; p (WT vs
599 HM)=0.001). (D) Survival curve showing that *depdc5*^{-/-} embryos have reduced survival with
600 most larvae dying around 14 dpf (N=2, n=15 per genotype). (E) Images showing that *depdc5*^{-/-}
601 larvae don't show gross morphological changes at 3 dpf. (F) Measurement of body length (upper
602 panel; n=20/genotype; p=0.0045 by unpaired Student's t-test) and eye size (lower panel;
603 n=12/genotype; p=0.7219 by unpaired Student's t-test) showed no significant change in either
604 parameter.

605

606 **Figure 2: *depdc5* knockout results in increased mTOR activity, hypoactivity, epileptiform**
607 **discharges and seizure susceptibility.** (A) Western blotting of 7 dpf larval lysates to examine
608 phospho-S6 levels in *depdc5*^{+/+}, *depdc5*^{+/-} and *depdc5*^{-/-} larvae showing hyperactivation of
609 mTOR signalling. (n=3; p(WTvsHT) = 0.0012; p(WTvsHM) = 0.0455). (B) Images of 6 dpf
610 *depdc5*^{+/+} and *depdc5*^{-/-} larval brains (transversal sections across the optic tectum)
611 immunostained with phospho-S6 antibodies and counterstained with DAPI. The panels on the
612 extreme right depict 3D reconstruction of single cells in *depdc5*^{+/+} and *depdc5*^{-/-} brains (Scale bars

613 from left to right panels: 20 μ m, 2.5 μ m, 1.5 μ m). (C) Spontaneous extracellular electrographic
614 activity recorded from the optic tectum of *depdc5*^{+/+} or *depdc5*^{-/-} larvae at 9 dpf showing
615 representative epileptiform activity of *depdc5*^{-/-} larvae displaying polyspiking discharges. (D)
616 Percentage of *depdc5*^{+/+} and *depdc5*^{-/-} larvae showing epileptiform activity in the brain (N=4;
617 n=10/genotype, Student's t-test p(WTvs HM)<0.0001). (E) Distance swam by 8 dpf larvae
618 across two 2 hour dark-4 hour light cycles. (F) Spontaneous coiling activity in 20 hpf embryos
619 monitored over 20 minutes represented as the percentage of total time during which the embryos
620 were active (N=3, n=20, Student's t-test p (WT vs HM)<0.0001). (G) Distance swam by 2 dpf
621 embryos upon exposure to 3mM PTZ represented as fold change compared to basal distance
622 swam by wildtype larvae at t₀. (N=3, n>10, student t-test, *: p<0.05) (H) Representative
623 swimming tracks of 2 dpf embryos during a 10-minute period following a 3mM PTZ exposure
624 (tracks of 3 replicates are shown in rows for each genotype).

625

626 **Figure 3: *depdc5* knockout alters gene expression in larval brains without affecting brain**
627 **morphology** (A) Volcano plot showing the differentially expressed gene expression profile
628 between *depdc5*^{+/+} and *depdc5*^{-/-} larval brains. See also Table S1. (B) Pathways showing high
629 enrichment in the differentially expressed genes (upregulated are shown in green,
630 downregulated, in red). (C) Whole mount images of *depdc5*^{+/+} and *-/-* larvae at different stages
631 of development immunostained with α -acetylated tubulin. (n>3/genotype/developmental stage;
632 Scale bar:40 μ m).(D) Measurement of head size and head surface area in 3 dpf *depdc5*^{+/+} and
633 *depdc5*^{-/-} larvae. (E) Whole mount images of 48 hpf *depdc5*^{+/+} and *-/-* larvae immunostained
634 with α -phosphorylated histone H3 (n>3/genotype). (F) Cresyl violet staining comparing 7 dpf

635 *depdc5*^{+/+} (top half) and *depdc5*^{-/-} (bottom half) larval heads showed no gross difference in the
636 density of cells in the brain. Scale bar=100 μ m.

637

638 **Figure 4: Defects in GABAergic networks in *depdc5* knockout zebrafish brains.** Images of
639 transverse sections of 6 dpf *depdc5*^{+/+} and *depdc5*^{-/-} embryos immunostained with GAD65/67
640 (A), gephyrin (C) and Nlgn2 (D) antibodies and counterstained with DAPI. Section level is
641 displayed in the schematic drawing. Regions indicated in red boxes have been magnified to show
642 the branching defects (N=3, n=3 embryos/genotype). Scale bar: 10 μ m. (B) Imaris-reconstructed
643 3D image with Gad65/67 positive GABAergic boutons shown in green projecting towards the
644 nucleus (DAPI) shown in blue. (Scale bar=2 μ m). (E) Images of longitudinal sections of 6 dpf
645 *depdc5*^{+/+} and *depdc5*^{-/-} embryos immunostained with parvalbumin 7 antibody (Scale
646 bar=25 μ m). Field of view is displayed in the schematic drawing (F) Quantification of the number
647 of GAD65/67-positive neurofilaments, gephyrin-positive puncta and parvalbumin-positive cells
648 in *depdc5*^{+/+} and ^{-/-} larval brain sections (N=3, n>3 embryos/genotype).

649

650 **Figure 5: Rescuing effect of GABA and rapamycin on *depdc5* knockout zebrafish.** (A)
651 Swimming activity of 8 dpf larvae, with the activity of *depdc5*^{+/+} larvae normalized to 100%
652 shows that treatment with GABA (100 μ M) can completely rescue hypoactivity (N=2,
653 n=20/genotype/treatment). Rapamycin treatment (100 nM from day 0-2, 300 nM from day 3
654 onwards) was used as a positive control. (B) Spontaneous coiling activity in 20 hpf embryos
655 shows that the hypoactivity of *depdc5*^{-/-} embryos is rescued by treating with 100 nM rapamycin
656 or with 100 μ M GABA from single-cell stage (N=2, n=20/genotype/treatment, Student's t-test p
657 (Control WT vs HM) <0.0001:****). Coiling activity of *depdc5*^{+/+} was set at 100% for each

658 sample, and the relative activity of the *depdc5*^{-/-} larvae is represented. (C) Western blotting of 9
659 dpf larval lysates to examine phospho-S6 levels in *depdc5*^{+/+} and *depdc5*^{-/-} larvae treated with
660 DMSO or rapamycin (100 nM from day 0-2, 300 nM from day 3 onwards) shows inhibition of
661 mTOR signaling upon rapamycin treatment. (D) Distance swam by 2 dpf larvae treated with
662 GABA (100µM) or rapamycin (100nM) upon PTZ exposure (3mM) (N=3, n>10). (E)
663 Representative swimming tracks of 2 dpf embryos (untreated or treated with GABA or
664 rapamycin) during a 10-minute period following PTZ exposure (3mM). (F) Images of transverse
665 sections of 7 dpf GABA treated *depdc5*^{+/+} and *depdc5*^{-/-} larval brains immunostained with α -
666 GAD65/67 and counterstained with DAPI. Regions indicated in red boxes have been magnified
667 to show the branching defects. GABA treatment (100 µM) was begun at 8 hpf (n=3
668 embryos/genotype). (G) Quantification of the number of GAD65/67 positive neurofilaments in
669 GABA-treated *depdc5*^{+/+} and *-/-* larval brain sections showing that GABA treatment does not
670 rescue the defects in *depdc5*^{-/-}. (H) Survival curve showing that treatment of *depdc5*^{-/-} larvae
671 with rapamycin (100 nM from day 0-2, 300 nM from day 3 onwards) first prolongs lifespan as
672 long as rapamycin is supplemented to the water (till day 20-shaded). Withdrawal of rapamycin
673 results in a drop in survival and all the larvae die by day 35. On the contrary, treatment with 100
674 µM GABA from 8 hpf doesn't extend survival. Both rapamycin and GABA did not affect
675 *depdc5*^{+/+}.

676

677 **Figure 6: Paracrine compensation by GABA and modulation of multiple independent**
678 **pathways in *depdc5* knockout zebrafish.** (A) Swimming activity of 8 dpf larvae treated with
679 muscimol (100 µM), baclofen (100 µM), a combination of both or vigabatrin (5 mM) with the
680 activity of *depdc5*^{+/+} larvae normalized to 100% shows that treatment with vigabatrin can

681 completely rescue hypoactivity, while GABA receptor agonists cannot. (B) Vigabatrin treatment
682 completely rescues PTZ-hypersensitivity of 2 dpf *depdc5*^{-/-} embryos (N=2, n>30; student t-test,
683 *: p value <0.05). (C) Overlap between gene expression datasets from *depdc5*, *gabral*, *tsc2* and
684 *scn1a* mutants. See also Tables S2 and S4. (D) A representation of the common pathways (axon
685 guidance and GABA synapse) affected in *depdc5* and *gabral* knockout brains with the common
686 genes indicated. See also Table S3.

687

688 **Figure 7: mTOR deregulation and GABAergic defects are independent effects of Depdc5**

689 **knockout.** (A) Western blotting of 7 dpf *depdc5*^{+/+} and *depdc5*^{-/-} larval lysates shows no
690 change in phospho-S6 levels upon GABA treatment (100 μ M from 8 hpf; top panel). Western
691 blotting of 7 dpf *gabral*^{+/+} and *gabral*^{-/-} larval lysates shows no difference in mTOR signaling
692 upon knocking out *gabral* (bottom panel). (B) Images of transverse sections of 7 dpf rapamycin
693 treated *depdc5*^{+/+} and *depdc5*^{-/-} larvae immunostained with α -GAD65/67 and counterstained
694 with DAPI. Section level is displayed in the schematic drawing. Regions indicated in red boxes
695 have been magnified to show the branching defects. Rapamycin treatment was begun at 8 hpf:
696 100 nM from day 0-2, 300 nM from day 3 onwards (n=3/genotype). Scale bar=10 μ m. (C)
697 Quantification of GAD65/67 positive neurofilaments in rapamycin treated *depdc5*^{+/+} and ^{-/-}
698 larval brain sections shows that rapamycin treatment does not rescue the reduced number of
699 filaments in *depdc5*^{-/-}. (D) Western blotting of 5 dpf larval lysates upon treatment with
700 increasing concentrations of rapamycin (50 nM, 250 nM, 500 nM, 1 μ M and 2.5 μ M) from 8 hpf
701 to estimate phospho-S6 levels shows a dose-dependent decrease. Rapamycin-containing water
702 was changed everyday. (E) qRT-PCR based estimation of some down- and upregulated genes
703 involved in axon guidance, GABA synapse and metabolism. *efla* expression was used for

704 normalization, expression of *depdc5*^{+/+} was normalized to 1. (p<0.05:*; p<0.01:**). (F)
705 Swimming activity of 7 dpf *tsc2* larvae treated with rapamycin and GABA (day 0 onwards) over
706 5 minute light-10 minute dark phases, with the activity of *tsc2*^{+/+} larvae normalized to 100%
707 shows that rapamycin, but not GABA can rescue the hypoactivity (Student's t-test
708 p<0.0001:****).

709

710

711 **STAR methods:**

712 **Contact for reagent and resource sharing**

713 Further information and requests for resources and reagents should be directed to and will be
714 fulfilled by the Lead contact: Éric Samarut (eric.samarut@umontreal.ca)

715

716 **Experimental model and subject details**

717 Routine zebrafish (*Danio rerio*) maintenance was performed following standard procedures
718 (Westerfield) at 28.5⁰C under 12/12 hour light/dark cycles at the animal facility of the Centre
719 Hospitalier de l'Université de Montréal Research Centre (CRCHUM), Montréal. All experiments
720 were performed in compliance with the guidelines of the Canadian Council for Animal Care. The
721 primary model used for this study was *depdc5* loss of function mutants.

722 For generation of the *depdc5* loss of function model, zebrafish optimized Cas9 mRNA was
723 synthesized using the mMESSAGING mMACHINE SP6 kit (Ambion) and a pCS2-nCas9n
724 template linearized with NotI. The following gRNA sequence targeting the 14th exon of *depdc5*
725 was designed using the online tool CRISPRscan (PAM site is indicated in brackets): 5'-
726 TGAGGATCATGAGCAAT(CGG)-3'. Synthesis of gRNA and of Cas9 mRNA was performed

727 as described [42]. Briefly, a 52 nt oligo (sgRNA primer), containing the T7 promoter, the 20 nt
728 of the specific sgRNA DNA binding sequence and a constant 15 nt tail for annealing, was used
729 in combination with a 80 nt reverse oligo to add the sgRNA invariable 3' end (tail primer). A 117
730 bp PCR product was generated following these parameters: 3 minutes at 95°C, 30 cycles of 30
731 seconds at 95°C, 30 seconds at 45°C and 30 seconds at 72°C, and a final step at 72°C for seven
732 minutes. PCR products were purified using Qiaquick (Qiagen) columns and approximately 120–
733 150 ng of DNA were used as template for a T7 In vitro transcription (IVT) reaction
734 (AmpliScribe-T7-Flash transcription kit from Epicentre). In vitro transcribed sgRNAs were
735 DNase treated and precipitated with Sodium Acetate/Ethanol. Cas9 mRNA was in vitro
736 transcribed from DNA linearized by *XbaI* using the mMachine T3 kit (Ambio). *In vitro*
737 transcribed mRNAs were purified by phenol-chloroform followed by isopropanol precipitation.
738 Tubingen long fin (TL) wild-type embryos were collected for microinjection. A 1nL drop of a
739 mix of 100 ng/μL of Cas9 mRNA and 30 ng/μL of gRNA was injected into one-cell stage
740 embryos using a Picospritzer III pressure ejector.

741 Genotyping of *depdc5*^{+/+} (wild type), ^{+/-} (heterozygous) and ^{-/-} (homozygous) animals
742 was performed by high resolution melting analysis (HRM) using genomic DNA extracted by
743 boiling the embryo/larva/clipped caudal fin in 50 mM NaOH for 10 minutes and then
744 neutralizing it with 100 mM Tris HCl (pH 8). HRM primers were designed using the Universal
745 Probe Library Assay Design Center (FP: 5' ATGCGCTGTTTGGTGAGG 3' and RP: 5'
746 TCCAGGAGTGGGTGTTTTTG 3'). All primer sets are available upon request. The PCR
747 reactions were made with 5 μL of the Precision Melt Supermix for HRM analysis (Bio-Rad
748 #172-5112), 0.5 μL of each primer (10 μM) and 2 μL of genomic DNA and water up to 10 μL.
749 The PCR was performed in a LightCycler 480 Instrument II (Roche) using white 96 well plates.

750 Two-step Evagreen PCR reaction protocol was 95°C for 2 min, then 45 cycles of 95°C for 10 sec
751 and 60°C for 30 sec, followed by 95°C for 30 sec, 60°C for 60 sec, the temperature was
752 increased by 0.02°C/sec until 95°C for 10 sec, then cooling at 40°C. Curves were analyzed using
753 the Roche LightCycler 480 software version 1.5.1.62.

754 In order to eliminate any putative off-target mutations, F0 founder was outcrossed with Tubingen
755 long fin wild-type fish for at least three generations before phenotyping the embryos. All
756 experiments were performed on larvae, and sex of zebrafish is not yet determined at this stage.
757 *depdc5*^{+/-} fish were incrossed to obtain *depdc5*^{+/+}, *depdc5*^{+/-} and *depdc5*^{-/-} from the same cross for
758 experiments. *depdc5*^{+/-} fish of different generations have been used to verify consistency of the
759 phenotype.

760

761 **Method details**

762 ***In situ* hybridization**

763 A specific probe for *depdc5* corresponding to the 5' part of the coding sequence and first exon
764 (971bp amplified with the following primers: FP: 5' TGACACAGAAAGTAGAGTTTGCAGG
765 3'; RP: 5' GTTCTCAGCATCTTTGGGAGC 3') was cloned within the pCS2+ vector using
766 TOPO TA cloning kit (Invitrogen). After sequencing, antisense probe was transcribed *in vitro*
767 using SP6 RNA polymerase. Whole-mount *in situ* hybridization of zebrafish embryos was
768 performed as described by Thisse et al., 2008 [43]. Stained embryos were kept in 80% glycerol
769 and imaged.

770

771 **Western blotting**

772 Larvae were anaesthetized and collected at 8 dpf, following which lysates were rapidly prepared
773 by homogenization in high salt lysis buffer containing 10 mM Tris HCl (pH 8), 20% glycerol,

774 0.4 M KCl, protease and phosphatase inhibitors. After a freeze-thaw cycle to ensure efficient
775 homogenization, the lysates were centrifuged at 13,000 rpm for 20 minutes. The supernatant was
776 collected, and protein concentration was estimated using Bradford assay (Biorad). Western
777 blotting was performed using 30 µg lysate per sample which were resolved on a 12% SDS-
778 polyacrylamide gel. After electrophoresis, proteins on the gel were electrotransferred onto 0.22
779 micron nitrocellulose membrane. The membranes were blocked with 5% non-fat milk solution in
780 1X phosphate buffered saline or with 5% bovine serum albumin (Sigma) in 1X Tris buffered
781 saline for immunoblotting with anti- γ -tubulin (#T6557; Millipore Sigma) or anti-total S6 (2217;
782 Cell Signaling Technologies) and anti-phospho S6 (#2215; Cell Signaling Technologies)
783 respectively. Detection was performed using goat anti-mouse and goat anti-rabbit antibodies
784 respectively conjugated with horse radish peroxidase. Bands were visualized with ECL and
785 imaged using ChemiDoc (Biorad).

786

787 **Non-invasive local field potential (LFP) recordings**

788 Non-invasive recordings reading the electric signal from the head of the larvae were performed
789 based on a modified protocol [19]. The larva was immobilized in 2% low melting point agarose
790 (Invitrogen). Recording electrode (soda lime glass, Hilgenberg, Germany) was pulled with a
791 DMZ Universal Puller (Zeitz, Germany) to a diameter of approximately 20 microns and filled
792 with artificial cerebrospinal fluid (ACSF, 124 mM, NaCl, 2 mM KCl, 2 mM MgSO₄, 2 mM
793 CaCl₂, 1.25 mM KH₂PO₄, 26 mM NaHCO₃ and 10 mM glucose). The differential signal between
794 the recording electrode positioned on larva's head above the optic tectum and the reference
795 electrode was amplified 10,000 times by DAGAN 2400 amplifier (Minnesota, USA), band pass
796 filtered at 0.3-300 Hz and digitized at 2 kHz via a PCI-6251 interface (National Instruments,

797 UK) with WinEDR (John Dempster, University of Strathclyde, UK). The duration of each
798 recording was 10 minutes. Epileptiform events consisted of multispikes with amplitudes
799 exceeding at least three times baseline and lasted for minimum 100 msec. Electrophysiological
800 recordings were analysed using Clampfit 10.2 software (Molecular Devices, USA).

801

802 **Motor activity measurements**

803 20 hpf embryos were embedded in low melting agarose and their movements inside the chorion
804 were recorded using a camera for 20 minutes during which time they were kept hydrated. The
805 Danioscope software (Noldus) was then used to quantify the percentage of time the embryos
806 were active, the number of bursts and burst duration. At later stages (>5dpf), larvae were
807 transferred individually into a 96-well plate and activity was recorded over light-dark cycles
808 using Basler GenIcam camera and DanioVision recording chamber (Noldus). Analysis was
809 performed using the Ethovision XT 12 software (Noldus) to quantify the distance swam.

810

811 **Drug treatment**

812 Drugs were procured from Sigma-Aldrich and LC Laboratories and stock solutions were
813 prepared (PTZ-300mM, GABA-100 mM, Muscimol-30 mM, Baclofen-15 mM, Vigabatrin-1M
814 in water and rapamycin-500 μ M in DMSO). Embryos were treated from 8 hpf unless mentioned
815 otherwise. The water was replaced everyday with fresh water containing final concentration of
816 the drug, till the activity measurement or end of the survival curve whichever was later. For PTZ
817 assay, manually dechorionated 2 dpf embryos were placed in a 96-well plate and let
818 accommodated for 20-30 minutes. PTZ from stock solution (300mM) was diluted to the final

819 concentration (3mM) directly in the wells and the embryos were tracked immediately during 20
820 minutes using a Daniovision (Noldus).

821

822 **Transcriptomic, differential expression and pathway analyses**

823 Three independent batches of 10 dpf *depdc5*^{+/+} and *-/-* larvae were dissected to extract the
824 whole brain, by each of two experimenters, corresponding to experimental triplicates. Total RNA
825 was extracted from these flash frozen brains using PicoPure RNA extraction kit (Thermo Fisher
826 Scientific) following the manufacturer's standard protocol. For each sample, RNA extraction
827 was made from 5 whole brains. Absence of contamination was assessed by Nanodrop using
828 260/280 and 260/230 ratios. Quality of total RNA was assessed with the BioAnalyzer Nano
829 (Agilent) and all samples had a RIN above 9.

830 Library preparation was performed using the Truseq RNA (Illumina). 13 PCR cycles were
831 required to amplify cDNA libraries. Libraries were quantified by Nanodrop and BioAnalyzer.
832 All libraries were diluted to 10 nM and normalized with the Miseq SR50 v2. Libraries were
833 pooled to equimolar concentration and multiplexed by 6 samples per lane. Sequencing was
834 performed with the Illumina Hiseq2000 using the SBS Reagent Kit v3 (100 cycles, paired-end)
835 with 1.6 nM of the pooled library. Cluster density was targeted at around 800k clusters/mm².
836 Between 45 and 55 million reads were generated for each sample. Library preparation and
837 sequencing was done at the genomics platform of the Institute for Research in Immunology and
838 Cancer (University of Montreal). About 90% of high quality reads were mapped onto the zv9
839 version of the zebrafish genome (ensemble release 77) using TopHat version 2.0.10.

840 Differential gene expression analysis was assessed by DeSeq2 package using R software. Genes
841 showing an absolute fold change >1.4 and adjusted p value <0.05 were considered to be

842 significantly differentially expressed. Pathway analysis was performed using DAVID
843 bioinformatics resources [44]. The list of differentially expressed genes was uploaded onto
844 DAVID analysis wizard and a list of all expressed genes found in our dataset was used as a
845 background for gene enrichment analysis.

846

847 **qRT-PCR**

848 400 ng of RNA extracted as described above was used for reverse transcription to prepare cDNA
849 with the Superscript VILO cDNA synthesis kit. The cDNA was diluted 1:10 and used for qPCR
850 with SYBR Green I Master (Roche) on a LightCycler 480 instrument. *ef1a* was used as the
851 reference gene for normalization. Primers were designed using the Roche Universal Library
852 Design Center online tool: gabrg2_F: cattcgtgtcctctcgagttc, gabrg2_R: agctgcgcttccacttgat;
853 kcc2_F: tggagccatgtacatcttgg, kcc2_R: tggcagctgatggaacaat; gat3_F: tgaacagaacgtgccatag,
854 gat3_R: cgctataaacgctagaccagga; plxn2a_F: agagcaaaaaccatcccaaa, plxn2a_R:
855 gcattctctcagcgacagact; sema3b_R: caacatggaccagcaactga, sema3b_R: ccattgcattcatctcgtc;
856 efnb3b_F: ctacacagggcatgaaggtg, efnb3b_R: ggagattggctggcaga; mt-cyb_F:
857 tgacttattcggagcatcca, mt-cyb_R: tagtctctgggcatgtg; mt-co2_F: gaaattaatgacccccacgttac, mt-
858 co2_R: cgtagcttcagtaccattgatgtc; ef1a_F: gtggctggagacagcaaga, ef1a_R: agagatctgaccaggggtggt.

859

860 **Immunostaining**

861 *depdc5*^{+/+} and *depdc5*^{-/-} embryos were anaesthetized in 0.2% tricaine, fixed with 4%
862 paraformaldehyde, cryoprotected in 10% sucrose overnight, and embedded in 7.5% gelatin/10%
863 sucrose solution prior to flash freezing in isopentane. Samples were stored at -80°C until use.
864 Embryos were cut into 20-µm-thick sections on cryostat, mounted on superfrost slides, and

865 stored at -80°C . For gephyrin immunostaining, *depdc5*^{+/+} and *depdc5*^{-/-} embryos were
866 embedded in OCT and frozen in liquid nitrogen. Cryosections (20 μm) were fixed in 4%
867 paraformaldehyde at room temperature for 10 min. After washing thrice with PBS, sections were
868 treated with 0.25% trypsin in 1X PBS for 2 min at 25°C . Immunohistochemistry was performed
869 as previously described [45]. Briefly, sections were blocked and permeabilized with 0.2%
870 gelatin, 0.25% Triton X100 diluted in 1X PBS for 1 hour at room temperature and then incubated
871 overnight at room temperature with anti-GAD65/67 (1:500, rabbit polyclonal, Ab11070,
872 Abcam), anti-Neurologin 2 (Nlgn2) (1:300, rabbit polyclonal, Ab 36602, Abcam), or anti-
873 gephyrin (1:100, rabbit polyclonal, ab185930, Abcam). After several washes, sections were
874 incubated for 1 hour with the donkey anti-rabbit coupled to Alexa Fluor 488 (1:500, Jackson
875 Laboratories, West Grove, PA). Sections were counterstained for 10 minutes with 0.1% DAPI
876 (Sigma-Aldrich) before being mounted with Vectashield Mounting Medium (Vector). Sections
877 were analysed using a Leica TCS SP8 confocal scanning system (Leica Microsystems). Eight-
878 bit-digital images were collected using a Leica 40x HCPL APO CS2 oil-immersion objective
879 (numerical aperture 1.30). Full-slices were captured 60-65 z-stacks, with a z step of 0.3 μm .
880 Images were processed with ImageJ software (National Institutes of Health, USA).

881 For whole mount immunostaining, *depdc5*^{+/+} and *depdc5*^{-/-} embryos were anaesthetized in
882 0.2% tricaine, fixed in Dent's fixative (80% methanol and 20% DMSO) overnight. After
883 rehydrating gradually into PBS, the larvae were permeabilized for 7 minutes in cold acetone.
884 Larvae were blocked and permeabilized with 2% normal goat serum, 2% BSA and 1% DMSO
885 diluted in 1X PBS for 1 hour at room temperature and then incubated overnight at 4°C with anti-
886 acetylated tubulin (1:500, mouse monoclonal, Abcam) or anti-phosphorylated histone H3 (1:500,
887 rabbit polyclonal, Millipore). After several washes, sections were incubated for 2 hours with the

888 goat anti-rabbit or goat anti-mouse coupled to Alexa Fluor 488. After washing, the fluorescence
889 was analyzed by confocal microscopy (Olympus BX61W1 equipped with a Quorum Technology
890 spinning disk head connected to a Hamamatsu ORCA-ER camera). Images were analysed using
891 Volocity software (Improvision).

892

893 **Cresyl violet staining**

894 *depdc5*^{+/+} and *-/-* embryos were anaesthetized in 0.2% tricaine, fixed with 10%
895 paraformaldehyde, embedded in paraffin, and sectioned. After deparaffinization and
896 rehydradation, slides were stained with 0.5% cresyl violet (Sigma; in 0.3% acetic acid). Sections
897 were differentiated in 70% ethanol and dehydrated in 100% ethanol. After clearing in xylene,
898 coverslips were mounted using Pertex mounting medium (HistoLab, Gothenburg, Sweden). The
899 slices of embryos were photographed with a microscope Nikon Eclipse (E-200) equipped with a
900 digital sight (Nikon).

901

902 **Morphological analysis**

903 3 dpf *depdc5*^{+/+} and *-/-* larvae were anaesthesized and dorsal and lateral images of the whole
904 body were acquired using the same parameters for all larvae. Body length, eye size, head size
905 and surface area were measured using the Danioscope software. Body length was measured from
906 the anterior tip to the caudal peduncle. Eye size and brain surface area were measured by
907 specifying the eye and brain boundaries.

908

909 **Quantification and statistical analysis**

910 **Quantification of gephyrin-labelled puncta and GAD65/67-labelled neurofilaments**

911 Apotome images from 20 μm sections labelled with anti-gephyrin were deconvoluted using
912 AutoQuant X (version X3.1.1) and processed using Image J (version 1.51s). Z-stacks were
913 manually contrasted to maximize synaptic puncta visibility and reduce background noise. Using
914 a semi-automatic macro, they were segmented by thresholding after filtering only synaptic
915 puncta with diameters varying from 0.15 to $2\mu\text{m}$ (macro written by Zsolt CSABA, INSERM
916 UMR1141). For each image, the total number of gephyrin-positive synapse puncta was divided
917 by the whole surface filled by these synapses to get the number of synapses per μm^2 . The ratios
918 of a total number of images from three independent experiments ($n(\text{depdc5}^{+/+})=9$; $n(\text{depdc5}^{-/-}$
919 $)=19$) were averaged to get the means and standard errors of the means (SEM) and assess
920 statistical tests between the two samples' groups.

921 For Gad65/67 quantification, 20 μm sections labelled with anti-GAD65/67 were imaged at zoom
922 6 using Leica HC PL APO CS 40X objective and processed using Bitplane Imaris (version
923 9.0.2). MeasurementPro's Filaments that detects automatically filament-like structures was used
924 to outline and quantify the dendrites. Images from three independent experiments
925 ($n(\text{depdc5}^{+/+})=3$; $n(\text{depdc5}^{-/-})=3$) were used to calculate the means and their standard errors
926 (SEM) and assess statistical tests between the two groups.

927

928 Quantification of morphological and locomotion parameters was performed using Danioscope
929 and Ethovision softwares respectively (Noldus) (described above). All data acquisition and
930 quantification was performed by experimenter blind to the genotype of the larva. There is no
931 evident morphological difference between *depdc5*^{+/+} and *-/-* which might bias the experimenter.
932 Details of biological and technical replicates, statistical test used and significance are mentioned
933 in the corresponding figure legend. All experiments have been repeated thrice on an average

934 (represented by N) and the number of animals per genotype used in each experiment is
935 represented by n. In most instances, unpaired Student's t test was performed to estimate
936 statistical significance. If $p > 0.05$, not significant, $p \leq 0.05$: *, $p \leq 0.01$: **, $p \leq 0.001$: *** and
937 $p \leq 0.0001$:****

938

939 **Data and software availability**

940 Complete list of significantly up- and downregulated genes ($p < 0.05$) in *depc5*^{-/-} larval brains in
941 comparison to *depc5*^{+/+} brains is available in Table S1. Complete list of genes overlapping
942 between the *depc5* and *gabral* datasets is available in Table S2. Table S3 has a list of common
943 genes between *depc5* and *gabral* datasets classified according to function. Table S4 gives the
944 complete list of genes overlapping between *depc5* and *tsc2* datasets.

945

946

947

948 **Supplemental file information:**

949

950

951 **Supplemental videos:**

952

953 **Video S1: 3D GAD65/67-labelled neurofilaments in *depc5*^{+/+} larval brains**

954 Reconstruction of 3D-images from fluorescent immunodetection of GAD65/67 accumulation
955 (green) on cryostat sections of 6 dpf *depc5*^{+/+} zebrafish embryos combined with DAPI
956 staining were imaged using confocal microscopy. Subsequently, z-stacks of selected region were
957 rendered into 3D volume using Imaris (Bitplane Inc.).

958 Related to figure 4.

959

960 **Video S2: 3D GAD65/67-labelled neurofilaments in *depc5*^{-/-} larval brains**

961 Reconstruction of 3D-images from fluorescent immunodetection of GAD65/67 accumulation
962 (green) on cryostat sections of 6 dpf *depdc5*^{-/-} zebrafish embryos combined with DAPI staining
963 were imaged using confocal microscopy. Subsequently, z-stacks of selected region were
964 rendered into 3D volume using Imaris (Bitplane Inc.).

965 Related to figure 4.

966

967

968 **Supplemental tables:**

969 **S1 Table: Complete list of significantly up- and downregulated genes in 10 dpf *depdc5*^{-/-}**
970 **larval brains in comparison to *depdc5*^{+/+} brains. Description of the top 5 up- and**
971 **downregulated genes is provided. Related to figure 3.**

972

973 **Table S2: List of common dysregulated genes between *depdc5* and *gabra1* datasets with the**
974 **fold change and pattern of deregulation. Related to figure 6.**

975

976 **Table S3: Common genes between *depdc5* and *gabra1* datasets classified according to**
977 **function. Related to figure 6.**

978

979 **Table S4: List of common genes between *depdc5* and *tsc2* datasets. Related to figure 6.**

980

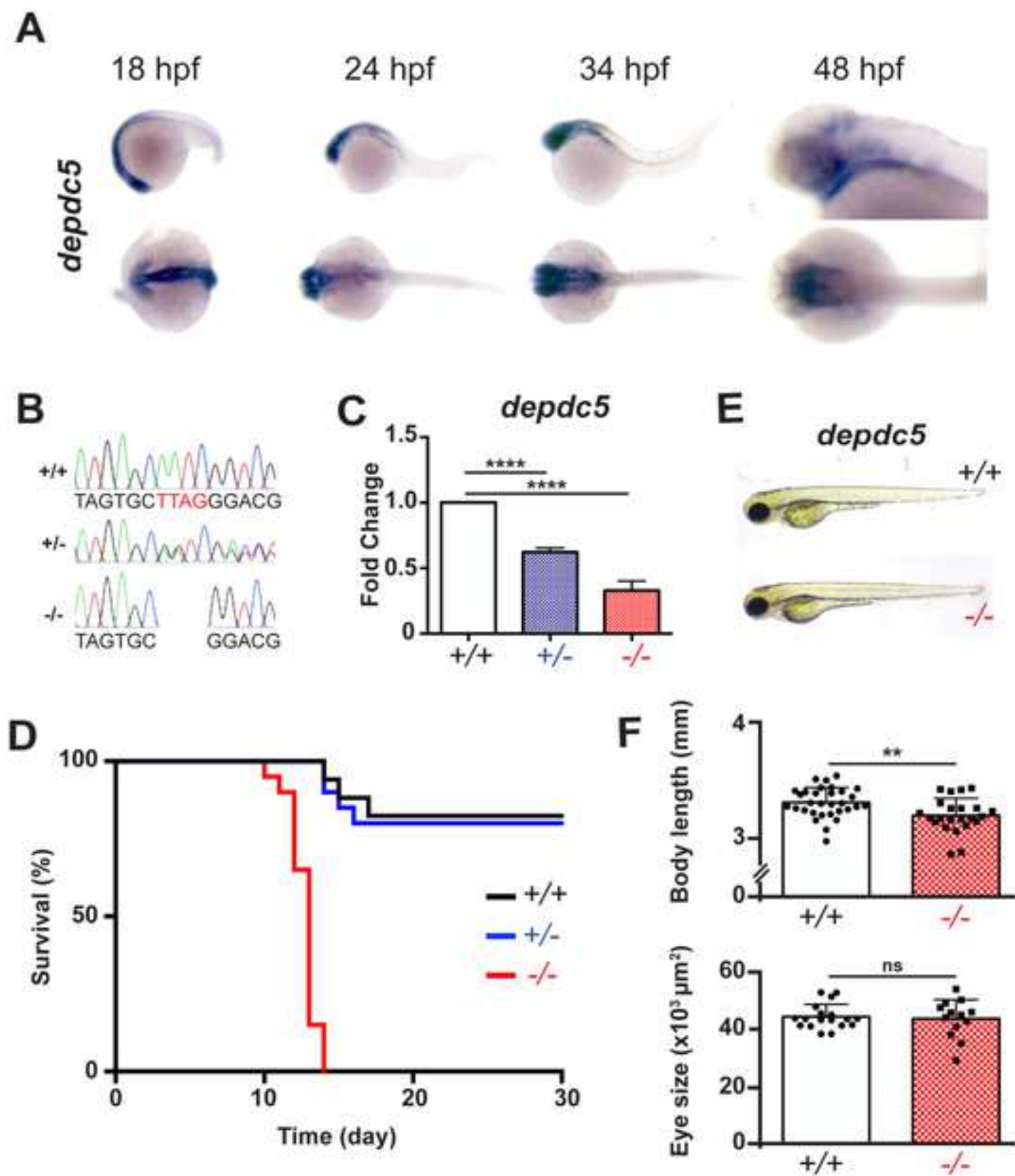
981

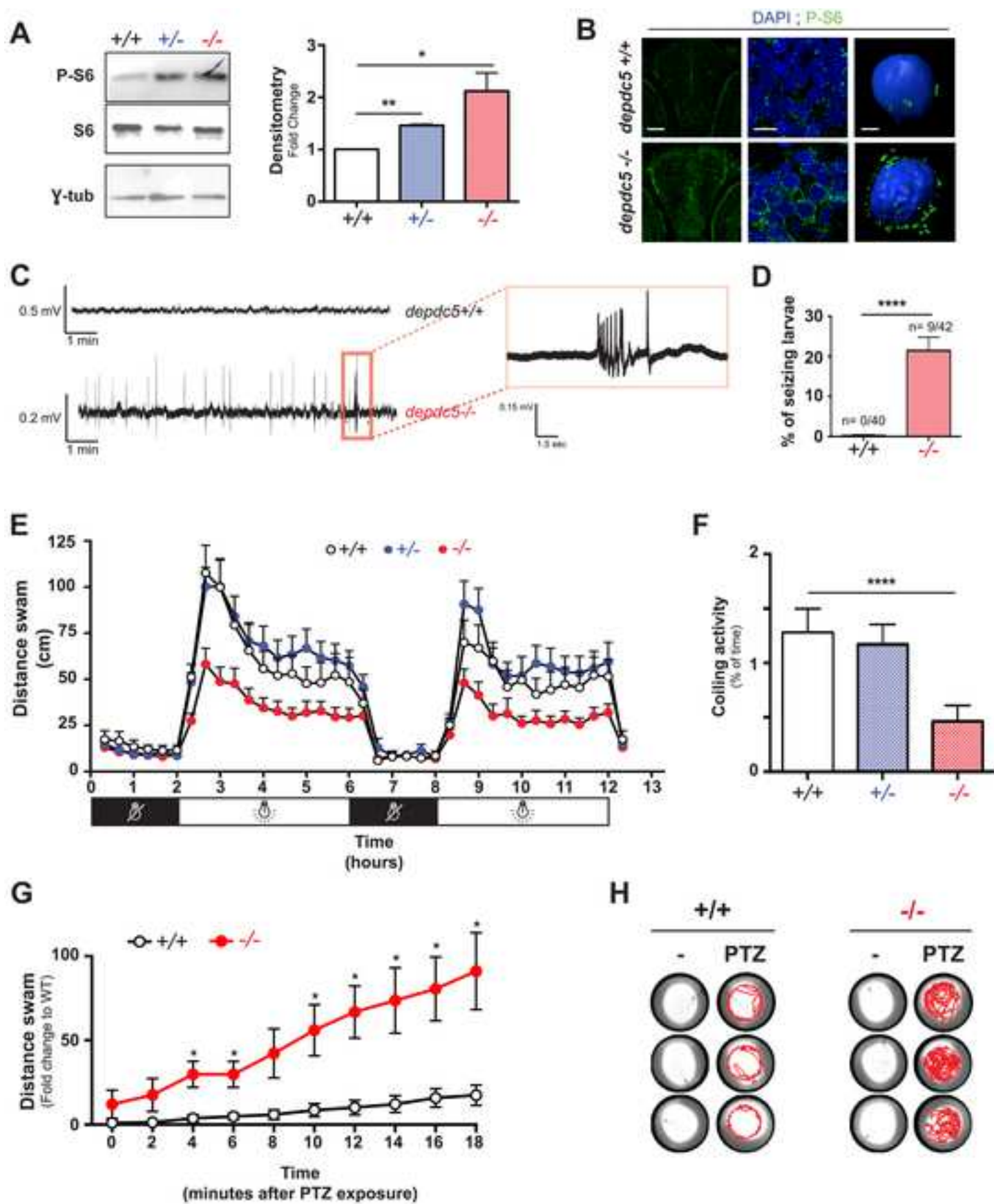
982

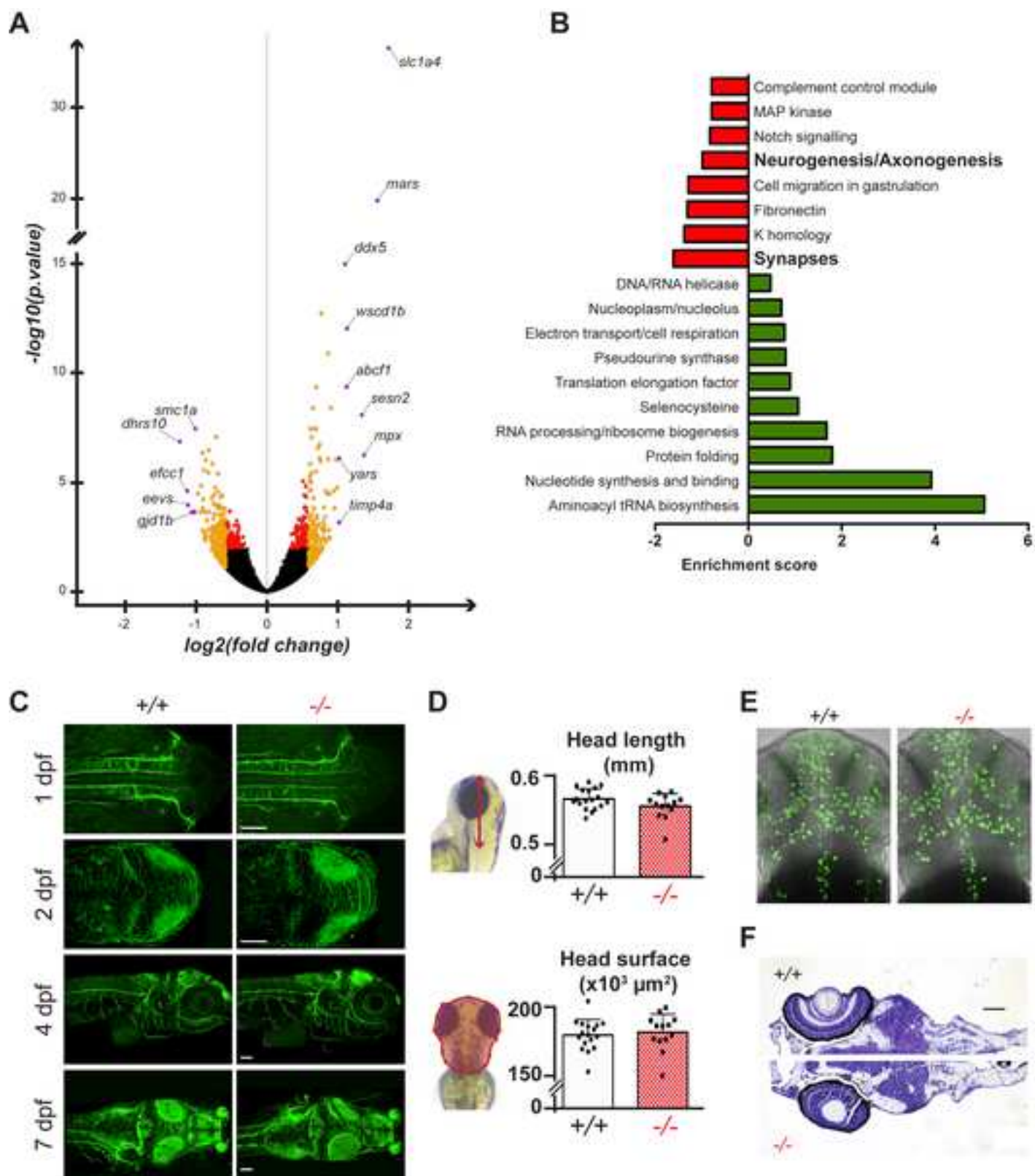
KEY RESOURCES TABLE

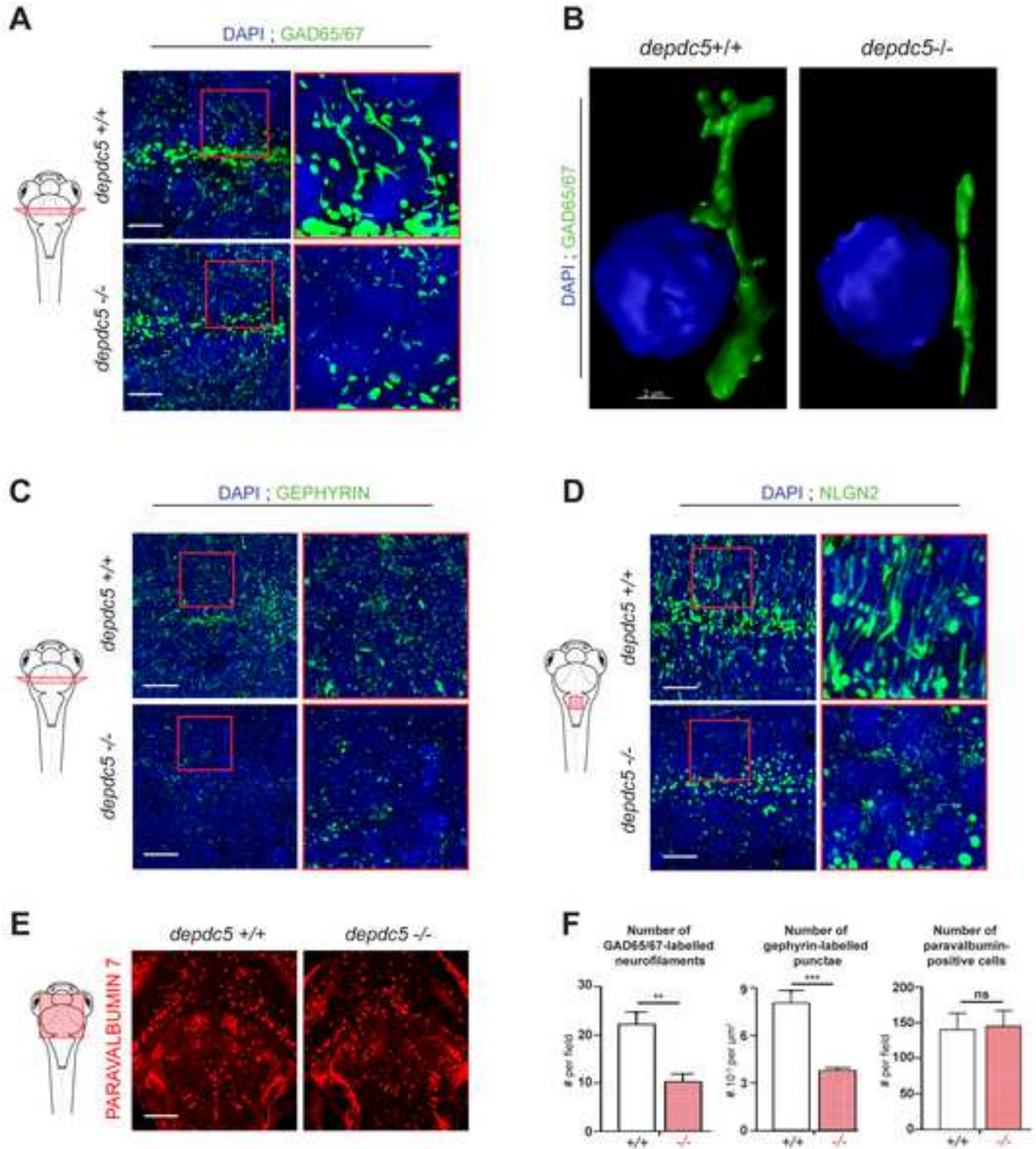
REAGENT or RESOURCE	SOURCE	IDENTIFIER
Antibodies		
GAD65/67	Abcam	Cat#Ab11070
Gephyrin	Abcam	Cat#Ab185930
Neuroigin 2	Abcam	Cat#Ab36602
Gamma-Tubulin	Millipore Sigma	Cat#T6557
Phospho histone H3	Millipore	Cat#09-838
Phospho ribosomal protein S6	Cell Signaling Technologies	Cat#2215
Ribosomal protein S6	Cell Signaling Technologies	Cat#2217
Acetylated tubulin	Sigma Aldrich	Cat#T7451
Bacterial and Virus Strains		
None	N/A	N/A
Biological Samples		
RNA extracted from 10 dpf larval brains of <i>depdc5</i> ^{+/+} , <i>+/−</i> and <i>−/−</i>	This manuscript	N/A
Chemicals, Peptides, and Recombinant Proteins		
<i>In situ</i> probe	Synthesized	N/A
Pentylentetrazol	Sigma	Cat#P6500
Cresyl violet	Sigma	Cat#190-M
Rapamycin	LC Laboratories	Cat#R-5000
GABA	Sigma	Cat#A2129
Vigabatrin	Sigma	Cat#V8261
Muscimol	Sigma	Cat#M1523
Baclofen	Sigma	Cat#B5399
Precision Melt Supermix for High resolution melting (HRM) analysis	Biorad	Cat#172-5112
Critical Commercial Assays		
mMESSAGE mMACHINE SP6 kit	Ambion	Cat#AM1340
TOPO TA cloning kit	Invitrogen	Cat#451641
PicoPure RNA extraction kit	Thermo Fisher Scientific	Cat#KIT0204
Superscript VILO cDNA synthesis kti	Invitrogen	Cat#11754050
Deposited Data		
<i>Tsc2</i> mutant zebrafish data	[20]	N/A
<i>Gabra1</i> mutant zebrafish data	Samarut et al (related manuscript, unpublished)	N/A
<i>Depdc5</i> mutant zebrafish data	This manuscript	N/A
Experimental Models: Cell Lines		
None	N/A	N/A

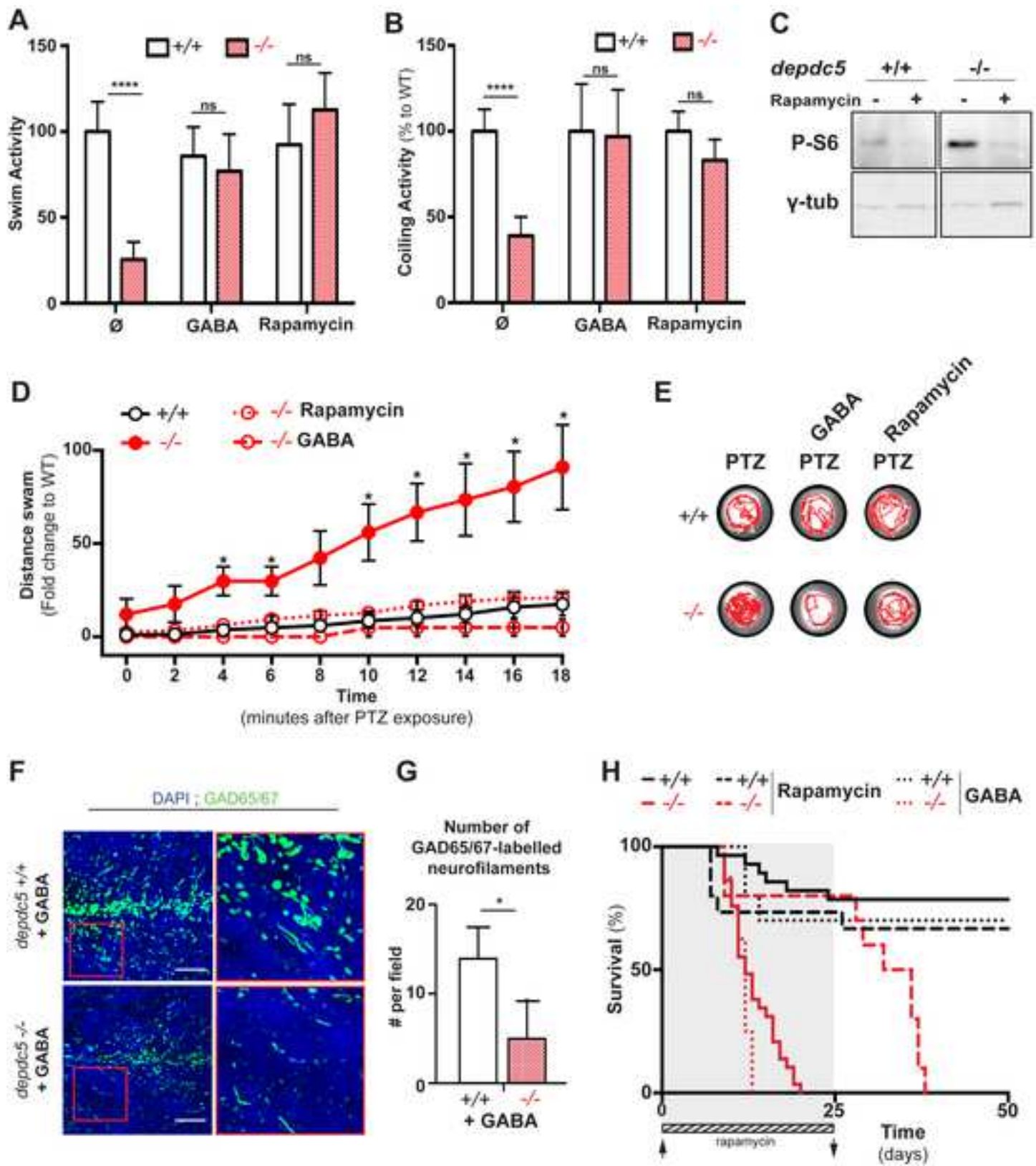
Experimental Models: Organisms/Strains		
Depdc5 loss of function mutant zebrafish	This manuscript	N/A
Tubingen long fin (TL) wild type zebrafish	ZIRC	ZIRC_ID: ZL86
Oligonucleotides		
Depdc5 HRM primers: sequence in methods	Sigma	N/A
Guide RNA targeting 14 th exon of <i>depdc5</i> (details of synthesis in methods)	This manuscript	N/A
qPCR primers for <i>depdc5</i> , GABA-related, axon-guidance related and metabolism-related genes: sequence in methods	Sigma	N/A
Recombinant DNA		
Plasmid encoding Cas9: pCS2-nCas9n	[42]	N/A
Software and Algorithms		
Danioscope	Noldus	Version 1.1 http://www.noldus.com/danioscope/more-about-danioscope
Ethovision XT	Noldus	XT12 http://www.noldus.com/EthoVision-XT/New
LightCycler 480	Roche	V1.5 https://lifescience.roche.com/en_ca/products/lightcycler14301-480-instrument-ii.html
Image J	NIH	V1.51 https://imagej.nih.gov/ij/download.html
R	The R project	V3.5.0 https://www.r-project.org
Volocity	Improvisation-Perkin Elmer	V3 http://cellularimaging.perkinelmer.com/downloads/detail.php?id=14
Imagelab	Biorad	V4.1 http://www.biorad.com/en-ca/product/image-lab-software?ID=KRE6P5E8Z
Other		

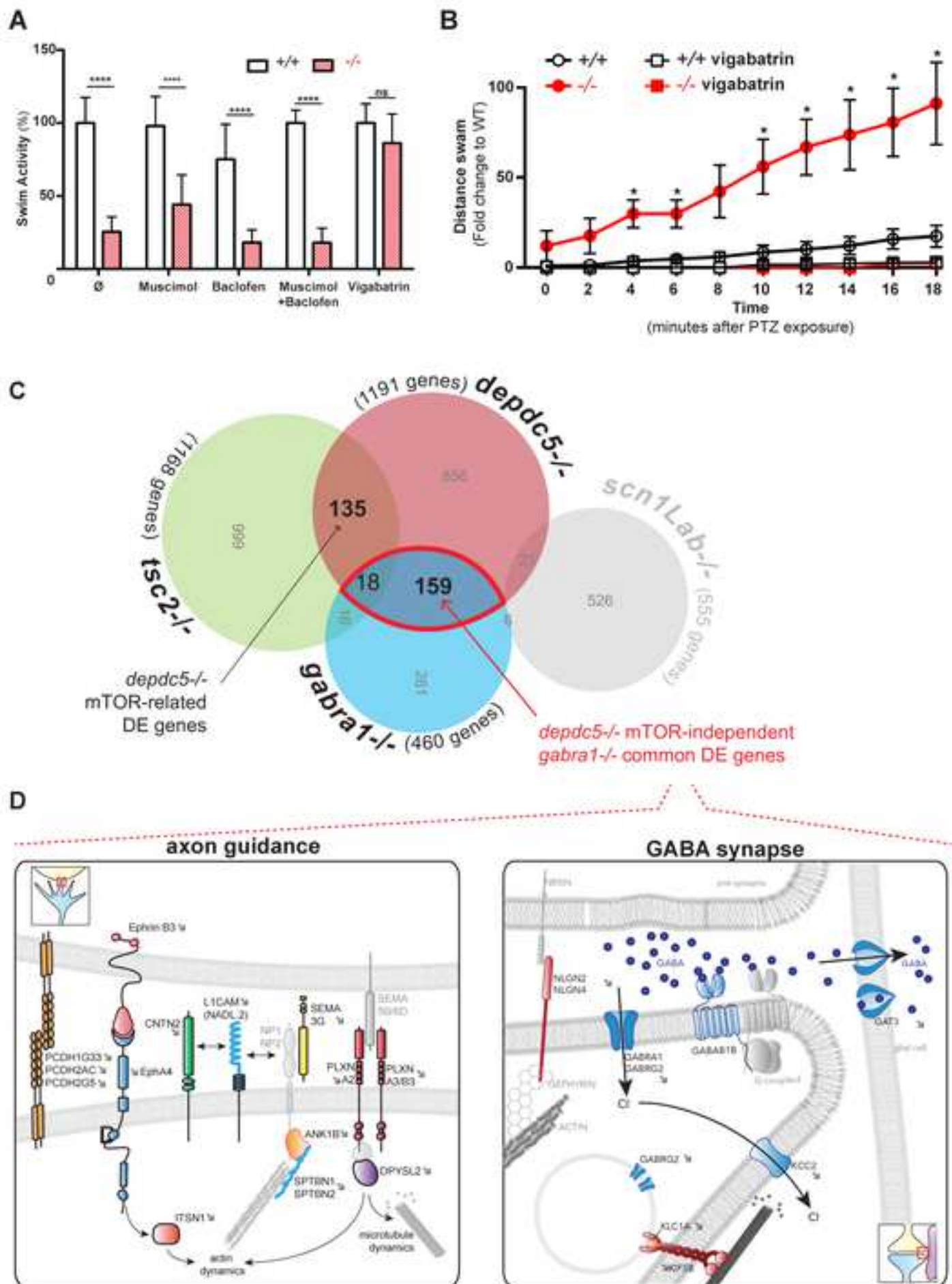


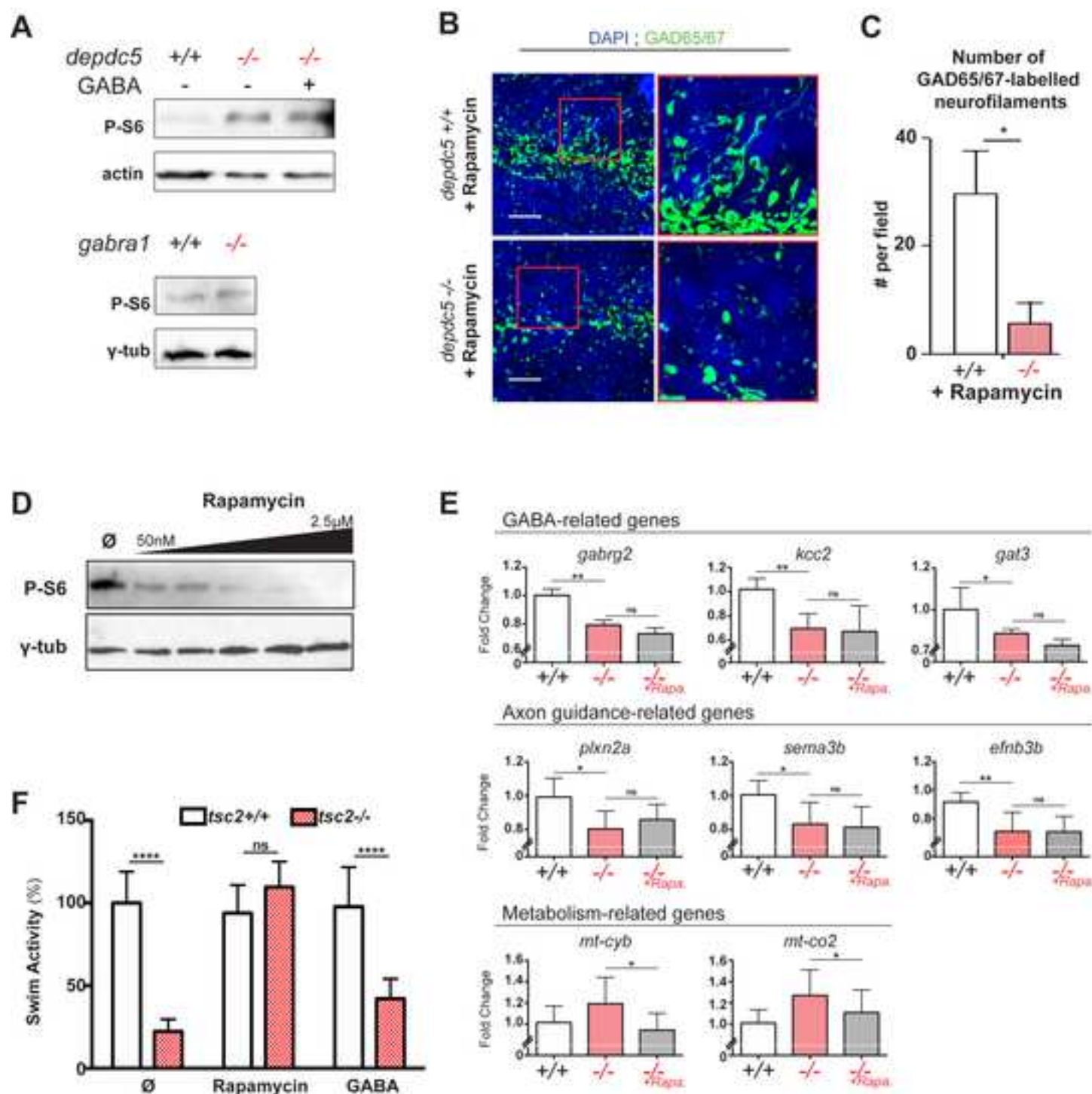








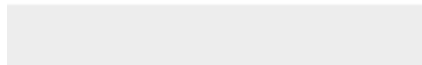
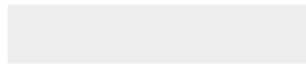






Click here to access/download

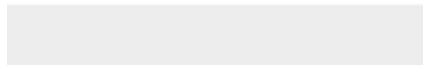
Supplemental Videos and Spreadsheets
Table S1.xlsx





[Click here to access/download](#)

Supplemental Videos and Spreadsheets
Table S2.xlsx





[Click here to access/download](#)

Supplemental Videos and Spreadsheets
Table S3.xlsx





Click here to access/download

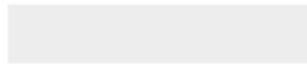
Supplemental Videos and Spreadsheets
Table S4.xlsx





[Click here to access/download](#)

Supplemental Videos and Spreadsheets
video S1.mp4





Click here to access/download

Supplemental Videos and Spreadsheets
video S2.mp4

